

See discussions, stats, and author profiles for this publication at: <https://www.researchgate.net/publication/355824632>

# Self-healing epoxy coating doped with *Elaeisis guineensis*/silver nanoparticles: A robust corrosion inhibitor

Article in *Construction and Building Materials* · December 2021

DOI: 10.1016/j.conbuildmat.2021.125396

CITATIONS

0

READS

12

6 authors, including:



**Mohammad Ali Asaad**  
Universiti Teknologi Malaysia

25 PUBLICATIONS 357 CITATIONS

[SEE PROFILE](#)



**Bothi Raja**  
Universiti Sains Malaysia

60 PUBLICATIONS 2,638 CITATIONS

[SEE PROFILE](#)



**Ghasan Fahim Huseien**  
National University of Singapore

113 PUBLICATIONS 1,349 CITATIONS

[SEE PROFILE](#)



**Roman Fediuk**  
Far Eastern Federal University

162 PUBLICATIONS 1,064 CITATIONS

[SEE PROFILE](#)

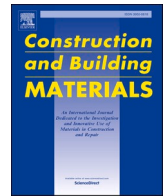
Some of the authors of this publication are also working on these related projects:



Feasible Use of Precast Foam Concrete composite Panel as a Load-Bearing Wall [View project](#)



Durability Properties of High-Strength Self-Compacting Ceramic Based Geopolymer Concrete [View project](#)



## Self-healing epoxy coating doped with *Elaeis guineensis*/silver nanoparticles: A robust corrosion inhibitor

Mohammad Ali Asaad<sup>a,\*</sup>, Pandian Bothi Raja<sup>b</sup>, Ghasan Fahim Huseien<sup>c</sup>, Roman Fediuk<sup>d</sup>,  
Mohammad Ismail<sup>e</sup>, Rayed Alyousef<sup>f,\*</sup>

<sup>a</sup> Department of Civil Engineering, Iraq University College, IUC Al-Estiqal St., Basra, Iraq

<sup>b</sup> School of Chemical Science, Universiti Sains Malaysia, Pulau Pinang, Penang 11800 USM, Malaysia

<sup>c</sup> Department of the Build Environment, School of Design and Environment, National University of Singapore, Singapore 117566, Singapore

<sup>d</sup> School of Engineering, Far Eastern Federal University, Vladivostok, Russian Federation

<sup>e</sup> Faculty of Civil Engineering, Universiti Teknologi Malaysia, UTM Johor Bahru, Johor 81310, Malaysia

<sup>f</sup> Department of Civil Engineering, College of Engineering, Prince Sattam Bin Abdulaziz University, Alkharij 11942, Saudi Arabia

### ARTICLE INFO

#### Keywords:

*Elaeis guineensis*  
EG/AgNPs inhibitor  
Self-healing  
Anti-corrosion  
MWCNTs

### ABSTRACT

This paper reports the self-healing properties of novel epoxy coating comprised of multi-walled carbon nanotubes (MWCNTs) as nanocontainers loaded with 5% green inhibitor-*Elaeis guineensis*/silver nanoparticles (EG/AgNPs) that acted as robust corrosion inhibitor for mild steel against adverse seawater environment. The self-healing assisted anti-corrosion effectiveness of the inventive coating for mild steel under seawater exposure for 42 days was evaluated via polarisation resistance, electrochemical impedance spectroscopy, adhesion strength and visual inspections. Further, the coated mild steel surface was characterised using X-ray diffraction, atomic force microscope and scanning electron microscopy analysis. The microstructures of smart powder (MWCNTs-EG/AgNPs) were also screened by a variety of microstructures techniques. Results revealed an excellent self-healing functionality of the produced smart epoxy coating with satisfactory anticorrosion behaviour against seawater exposure. A maximum of 97.87% inhibition efficiency and a minimum of 0.0009 mm/year corrosion rate were recorded after 42 days of exposure. Furthermore, this smart coating disclosed superior corrosion inhibition abilities even after 42 days of submersion in seawater by weakened the lepidocrocite ( $\gamma$ -FeOOH), as a result of the release of *Elaeis guineensis* /AgNPs, which in turn acted as efficient corrosion inhibitors to repair or self-heal the damaged coatings on mild steel surface.

### 1. Introduction

Since the human civilization, metals and its alloys remained the workhorse in the industrial and construction engineering sector due to their unique strength and ductility in addition to several other notable attributes. The applications of metal materials are very wide, including buildings, dams, casing, tubing, valves, tanks, pumps, boreholes, boilers, as well as bridges [1–5]. Despite such superior features, metals frequently become thermodynamically unstable and suffer from corrosion under diverse aggressive environments [6,7]. The main corrosive agents of those constructions are  $\text{Cl}^-$ ,  $\text{H}_2\text{O}$ ,  $\text{SO}_4^{2-}$ ,  $\text{H}_2\text{S}$ ,  $\text{CO}_2$ , and dissolved  $\text{O}_2$  [8–11]. Since metallic corrosion of expensive civil engineering structures causes billions of dollars economic loss annually on a global basis [12–14], safety reduction, pollution of the environment, and loss

of product [15], diverse approaches are developed to protect metal against corrosion.

These protection techniques include, shapes of the metal [16], electroplating [17], galvanizing [18], cathodic protection [19,20], insulating coatings [21,22] and corrosion inhibitors [23–26]. Epoxy coating technique is commonly exploited to circumvent the metal corrosion. In this technique, a coating on the metal is applied to create a dense barrier against corrosive elements [27,28]. These coatings prevent metal corrosion by maintaining the protective barrier. However, breaching of the barrier causes a quick development of the corrosion processes due to the association of varieties of additional reactions. This in turn may influence both the composition and properties of the metal surface and its immediate environment [29,30].

The degradation of epoxy coating may originate from various other

\* Corresponding authors.

E-mail addresses: [mohammad.asaad@iuc.edu.iq](mailto:mohammad.asaad@iuc.edu.iq) (M. Ali Asaad), [r.alyousef@psau.edu.sa](mailto:r.alyousef@psau.edu.sa) (R. Alyousef).

external factors including UV radiation, extreme temperature variation and mechanical cracks or scratches of the surface. All these effects leads to the opening of pores and crack propagation, thereby allows the movement of water and dissolved ions by capillary action, make contact with the metal surface, and eventually the initiation of corrosion [31–33]. Once the corrosion is commenced, the coating cannot defend the defective zone effectively and fails to prevent the defect propagation on the metal surface. To provide enduring corrosion protection, coatings with active “self-healing or smart” support are preferred. Such coatings can extend the interval required between maintenance inspections.

The ability of encapsulated inhibitors and sealants to interact with their environment together with sensing and response to appropriate changes may offer notable benefits including the reduction of human error, and misjudgement or negligence. Besides, it can simplify the overall operational costs [34,35]. Driven by this idea, lately the research on the development of nanocontainers has generated renewed interests. It is realized that such nanocontainers release corrosion inhibitors and thus make the coating susceptible to aggressive corrosion medium. The technology of encapsulating corrosion inhibitors that offer responsive nanocontainers, became prospective towards the development of self-healing protective coatings. Nanoparticulate fillers provide superior barrier properties even at low concentrations over conventional micron sized amendments [36]. Furthermore, most nanocontainers including halloysite nanotubes [37], silica tubes [38], cerium molybdate nanocontainers [39], and hollow core-shell nanoparticles [33], can only act as corrosion inhibitors releasing agents. They cannot optimise the other properties of coatings and may rather weaken the adhesion and structural characteristics.

Of late, carbon nanotubes (CNTs) became attractive owing to their multifaceted superior traits. According to Lee et al. [40], it is possible to exploit multiwall carbon nanotubes (MWCNTs) as optimum nano-materials for interfaces, particularly for controlling the boiling heat transfer. The superior thermal properties, good mechanical-chemical stability and optimum fibre-like structures to enhance porous layer production of MWCNTs make them a choice in its own right. Gergely et al. [41,42] were extensively screened CNT's role over zinc – rich hybrid paints application for low carbon steel corrosion against NaCl medium [42,43]; the series of reports include the characterization of nano-particles [41] and protection properties/mechanism of hybrid coatings [43]. They also [42] successfully tested the alkyl paint coatings embedded with alumina and CNT for the protection of cold-rolled steel in 1 M HCl and NaCl medium. Lanzara et al. [44] used CNTs as self-healing containers to significantly reduce the voids size in healed crack regions and hence structural reinforcement. Besides, improved adhesion and cohesion characteristics of coatings combined with MWCNTs have been reported by Park and Shon [45]. Shen et al. [46] have argued that CNTs could be conductive additives due to their optimal electrical conductivity and characteristic length-to-diameter (aspect) ratio. Although, a variety of filler inhibitors have been studied as self-healing amendments to provide enduring mild steel protection [47–53], literature revealed that so far very few studies have exploited the green nanotechnology route to synthesize self-healing filler as protective coatings of mild steel against aggressive corrosion medium. The green nanotechnology enroute production of metal nanoparticles is an emergent area with applications in physics, chemistry, biology, material science and medicine [54–58]. Presently, green nanotechnology is preferred to surmount the detrimental effects of heavy metals on human health and ecosystem. Environmentally-friendly, ‘green’ and inexpensive alternative coatings are demanded to minimise the excess usage of potentially toxic coating constituents [59–64]. Such green materials based coatings are advantageous because of superior chemical resilience, anti-bacterial abilities, catalytic, as well as electrical conductivity [65,66].

Although, majority of research over nanotechnology involves the synthesis and stabilisation of a range of nanoparticles by physical and chemical methodologies which are not environmentally sound, there is

now an increasing necessity to develop an environmentally friendly route involving non-toxic materials that do not contain heavy metals. Due to their diminutive size and their mechanical, electromagnetic, optical and biochemical properties [67], such nanoparticles can be used to inhibit corrosion of the metals when the composite material is exposed to aggressive species. Amongst the noble metallic particles, AgNPs-silver nanoparticles have enticed more regard as they possess a huge number of performances, including optical properties, high-efficiency, and unique electronic. This can be contributed to potential commercial applications in various areas, such as nanomedicine, electronics, catalysis, and optics [68–70].

With this plan, oil palm (*Elaeis guineensis*-EG) leaf extract was investigated as an alternative/advanced sustainable corrosion inhibitor for mild steel protection. The oil palm (EG) is a member of the *Arecaceae* family of plants. Malaysia is currently the second largest global palm oil producer with 4.917 million hectares under oil palm cultivation [71]. Whilst oil palm finds a variety of uses in plywood manufacture [72], cooking oils [73] and other food items [74], as well as in pharmacology [75], the leaf residues are considered an agricultural waste product. Hence, the utilisation of a corrosion inhibitor extracted from the (EG) plant, combined with a synthesis of silver nanoparticles (AgNPs) to produce a green nanoparticles corrosion inhibitory compound (EG/AgNP) encapsulated with MWCNTs applicable to mild steel in aggressive environments represents an innovative feature of this work.

Hefni et al. [76] studied the performance of Ch-g-mPEG inhibitor (chitosan (Ch) grafted with poly(ethylene glycol) on carbon steel in 1 M HCl solution in the presence and absence of AgNPs. The results revealed that the inhibition efficiency of Ch-g-mPEG/AgNPs inhibitor was 93% compared to 77% for Ch-g-mPEG inhibitor alone at the same concentration. Atta et al. [77] incorporated AgNPs into poly (vinyl pyrrolidone) matrix, and stated that the inhibition efficiency up to 91% was acquired. In brief, many researchers have successfully incorporated the inhibitors with silver nanoparticles, which found enhanced the inhibition efficiencies and reduced the corrosion rate of mild steel exposed to different aggressive environments [78–84].

Organic inhibitors tend to be mixed inhibitors, displaying both anodic and cathodic actions in tandem, and are exceptionally effective inhibitors due to the presence of heteroatoms such as oxygen, nitrogen and sulphur and the presence of multiple bonds in their molecules, all of which facilitate adsorption onto the metal surface [24,85,86]. According to Ali [87], they decrease the corrosion rate by: (i) increasing or decreasing the anodic and/or cathodic reaction, (ii) decreasing the rate of diffusion of reactants to the metal surface, and (iii) decreasing the electrical resistance of the metal surface.

Concern with all added advantages of smart/green coatings, we evaluated the corrosion protection ability of epoxy embedded MWCNT incorporated with EG/AgNPs inhibitor against mild steel corrosion in seawater. For determination of anti-corrosion efficacy of smart coating (epoxy coating embedded with MWCNTs incorporated with EG/AgNPs), mild steel surface was immersed in seawater for prolonged duration and subsequently monitored using potentiodynamic polarisation, electrochemical impedance spectroscopy (EIS), scanning electron microscopy (SEM), energy dispersive X-ray (EDX) spectroscopy, X-ray diffraction (XRD), atomic force microscopy (AFM), adhesion strength and visual observation test. Finally, the powder form of MWCNTs-EG/AgNPs (smart nanocontainers), as well as EG/AgNPs (inhibitor), were characterized via transmission electron microscopy (TEM), (XRD), field emission scanning electron microscopy (FESEM), thermogravimetric analysis (TGA) and EDX techniques.

## 2. Materials and methods

### 2.1. Preparation mild steel coupon

The mild steel sheet was mechanically cut into coupons in size of (40 mm × 30 mm × 1 mm), abraded by emery papers of grade up to 1500

particle size and then decreased with 70% acetone. Next, the mild steel coupon was rinsed with distilled water and air-dried prior to immersing in the coating. The mild steel coupon was composed of 0.5% of Si, 0.04% of S, 0.1% of Mn, 0.27% of C, 0.06% of P and 99.03% of Fe. For electrochemical analysis, both coated/non-coated mild steel specimens were prepared accordingly to fit over electrochemical cell with exposed area of 1 cm<sup>2</sup>. In order to study the self-healing properties of epoxy coating, mild steel specimens were scratched with X– mark (surface area ≈ 0.785 cm<sup>2</sup>) and the electrochemical data were normalized to 1 cm<sup>2</sup>.

## 2.2. Preparation of green nanoparticles inhibitor (EG/AgNPs)

The fresh leaves of *Elaeis guineensis* (palm tree) were manually collected from UTM- Universiti Teknologi Malaysia, Malaysia, to extract the EG inhibitor, the specimens were rinsed under running fresh water and left to dry in a place protected from light. Total phenolic contents (TPC) are reported to be higher in freeze and shade drying that gave the highest antioxidant capacity [88]. As far as simplicity and effective method is concerned, we have chosen a shade drying based on this literature. After drying, the leaves were turned into powder with 1–5 mm particles. This was followed by the suspension of 100 g of powder into 800 mL analytical reagent grade 95% ethanol (Qrèc) at temperature of 25 ± 3 °C for a period of 15 days (optimum time period). Afterward, the suspension was filtered through Whatman No.1 filtration paper before being subjected to Heating Mantle (MS-E105) to evaporate the ethanol extract. At last, the resultant 250 mL concentrated EG extract (EG extract and the rest of ethanol with a ratio of 1:2 respectively) was used for further study.

Silver ions (Ag<sup>+</sup>) were initially derived from silver nitrate (AgNO<sub>3</sub>) (Fluka, purity 99.99%) to synthesise EG/AgNPs. About 1000 mL of AgNO<sub>3(aq)</sub> (0.1 M) were added to 250 mL of *Elaeis guineensis* leaf extract in an Erlenmeyer flask at room temperature. The aqueous medium colour was changed immediately from dark-green to yellowish-green signalling the formation of AgNPs [61,62,89]. Next, the aqueous media were allowed to settle for 72 h (three days) at room temperature. AgNPs were extracted by centrifuging at 6000 rpm for 15 min and then allowed the reagents to dry. The green solid residues of EG/AgNPs were rinsed twice with double distilled water and redissolved in 95% ethanol which was finally evaporated. The cleaned and dry EG/AgNPs inhibitor powder, having an average size of 13.35 nm was used in the corrosion studies by incorporating into epoxy embedded MWCNTs.

## 2.3. Encapsulation of EG/AgNPs inhibitor into MWCNTs containers

MWCNTs containers (purchased from Cheap Tubes, USA) with outer diameter of 10–20 nm, electrical conductivity below 100 s/m, specific surface area of 233 m<sup>2</sup>/g, length of 10–30 μm, and density of 2.1 g/cm<sup>3</sup> was used. Green EG/AgNPs inhibitor powder was encapsulated with following the modified protocol of Kartsonakis et al. [90]. The MWCNTs containers were loaded with EG/AgNPs corrosion inhibitor powder wherein 8 g of EG/AgNPs powder was dissolved in 200 mL of (70% acetone, (RCI Labscan)) for 48 h to achieve a saturated solution. Then, 1 g of MWCNTs containers were placed in a sealed container and the air on the interior side of the MWCNTs containers were evacuated via a vacuum pump (Gast, Doap104BN Model) for 20 min so that air could be removed from the CNTs. Next, these containers were recycled at atmospheric pressure and the process was repeated three times to enhance the loading efficiency. It's noteworthy that the saturated EG/AgNPs was also present at this process. Afterward, the saturated solution comprising of EG/AgNPs inhibitor and MWCNTs were placed in the sealed container and the whole mixture was subjected to stirring for 2 h at room temperature using a hot plate stirrer with a stirring temperature of 60 °C (Favorit, HS070V2 Model). Finally, the MWCNTs containers encapsulated with EG/AgNPs were concentrated via centrifugation (Hettich, EBA 21 Model) for 15 min at the revolution of 6000 min/s before being oven (Mettmert, UF30 Model) dried at 50 °C for 5 h.

## 2.4. Preparation of Self-Healing coating

The epoxy material that used for the coatings was consisted of water-based epoxy system frequently utilised as anticorrosive primer and the epoxy material properties is listed in Table 1. Two sets of water-based epoxy solutions were prepared namely blank coating (without smart nanocontainers) and modified coating (with smart MWCNTs-EG/AgNPs nanocontainers (inhibitor-loaded MWCNTs containers). The smart MWCNTs-EG/AgNPs nanocontainers of concentration 5% (w/w) were added to the blank epoxy coating and the whole mixture was exposed to sonication for 24-hour, which is led to yielding a uniform dispersion of MWCNTs-EG/AgNPs in the coating without any precipitation. The epoxy mixture loaded with the smart MWCNTs-EG/AgNPs nanocontainers was applied to mild steel coupons by following the method reported elsewhere [91]. The procedure involved 30 s of dip-coating followed by drying at room temperature for 30 min together with baking in an air circulating oven at 50 °C for 4 h. Eventually, a coating with thickness range of 11.8–15.6 μm was achieved. The coated mild steel specimen was cooled and then deliberately scratched before being immersed in the seawater which was collected from Pontian Seaside, Johor, Malaysia. The scratch was made using a blade reached the mild steel surface, producing up to 430.2 μm wide scratches.

## 2.5. Electrochemical test

Potentiodynamic polarisation and EIS measurement was performed to evaluate the electrochemical performance of plain and coated mild steel (MS) with the blank coating, and the one modified with MWCNTs-EG/AgNPs subjected to seawater. The mild steel coupons were suspended in beakers that consist of 200 mL natural seawater. Electrochemical tests were conducted in a 3-electrode cell comprised of MS coupons as working electrodes with an exposed area of 1 cm<sup>2</sup>, a platinum wire having a surface area of 4.9 cm<sup>2</sup> as a counter electrode, in addition to saturated calomel (SCE) as a reference electrode. The electrochemical measurements were conducted utilising an electrochemical workstation VersaSTAT 3 (USA) at room temperature. The MS (plain/scratched coating) was submerged in the natural seawater test solution for 30 min until a steady state open-circuit potential (OCP) was developed and the corrosion progress was monitored after 7 days, 21 days and 42 days. The composition of the seawater used in this study is presented in Table 2. In order to analyse the electrochemical impedance results, ZSimpWin software was utilised over an equivalent circuit for fitting impedance data. EIS measurements were conducted at 10 mV-potential amplitude, peak to peak (AC signal) in an open circuit at 0.1 Hz–10,000 Hz - frequency range. The values for charge transfer resistance were determined from the Nyquist plots' using semicircular diameter. Meanwhile, DC polarisation studies were carried out over potential voltage from –250 mV to +250 mV with reference to the open circuit potential at 0.5 mV/s - scan rate. Extrapolation of the linear Tafel segments of anodic and cathodic curves to corrosion potential was performed to obtain the values of the corrosion current densities (*i*<sub>corr</sub>). The formulas below were used to determine the inhibition efficiency (IE) values for Tafel and EIS tests, respectively at various immersion times in the presence and absence of 5% EG/AgNPs inhibitor (utilised as an

**Table 1**  
Properties of water-based epoxy.

Parameter	Value
Appearance	Grey liquid
Viscosity	570 (cPs) @ 25 °C
Solid content (%)	80 ± 2
Density	1.1 g/cm <sup>3</sup> @ 23 °C
Temperature resistance	To 120 °C
Dry to touch	6 h @ 20 °C
Specific gravity	1.13 g/cm <sup>3</sup> @ 25 °C
Tensile Strength	6.85 MPa

**Table 2**  
Chemical compositions of seawater.

Chemical Ion	H <sub>2</sub> O	Cl <sup>-</sup>	Na <sup>+</sup>	Mg <sup>2+</sup>	p <sup>3-</sup>	SO <sub>4</sub> <sup>2-</sup>	Ca <sup>2+</sup>	K <sup>+</sup>	Rr <sup>-</sup>	Fe <sup>2+</sup>
Concentration(ppm)	979,000	14,400	6800	1100	870	715	420	310	61	4

optimum percentage):

$$IE(\%) = \left(1 - \frac{i_{\text{corr}}^{\text{inh}}}{i_{\text{corr}}^{\text{o}}}\right) \times 100\% \quad (1)$$

where  $i_{\text{corr}}^{\text{o}}$  denotes the corrosion current density without an inhibitor, while  $i_{\text{corr}}^{\text{inh}}$  denotes the corrosion current density in the presence of an inhibitor.

$$IE(\%) = \left(1 - \frac{R_{\text{ct}}^{\text{inh}}}{R_{\text{ct}}^{\text{o}}}\right) \times 100\% \quad (2)$$

where  $R_{\text{ct}}^{\text{inh}}$  and  $R_{\text{ct}}^{\text{o}}$ , the charge transfer resistance in the presence and absence of EG/AgNPs respectively.

## 2.6. Surface characterisation

### 2.6.1. SEM imaging

The morphology of the plain and coated mild steel surface (blank epoxy and epoxy modified with 5% of MWCNTs-EG/AgNPs) at scratched area were examined by SEM (Jeol, JSM-IT300) after immersing it in the seawater for 42 days. The coated mild steel coupon of dimension (30 mm × 40 mm × 1 mm) was gold covered for 90 s by automated platinum sputter coater (Qourum-Q150R Model) before being glued (using double-sided tape) on Aluminium stub of diameter 32 mm. In addition, the images of the coated mild steel coupons with and without MWCNTs-EG/AgNPs were formed by backscattered electrons.

### 2.6.2. AFM analysis

An AFM (Nano Wizard 3, JPK) technique was used to image the mild steel surface of dimension (30 mm × 40 mm × 1 mm) for blank epoxy coating and loaded with smart nanocontainers (MWCNTs-EG/AgNPs). A square area of (20 μm × 20 μm) on the mild steel surface was scanned at scan time of 0.5 s. The AFM instrument which is provided by a silicon cantilever (Nano ACCESS – NC – A) having a spring constant of 25–95 N/m, tip radius below 10 nm operated at a frequency range of 200–400 kHz.

### 2.6.3. XRD analysis

The XRD pattern was measured using model Rigaku, SmartLab 3 kW for analysing the composition of the corrosion products of mild steel surfaces at scratched area following immersing it in the seawater for 42 days. The mild steel surface of dimension (30 mm × 40 mm × 1 mm) for blank epoxy coating and loaded with smart nanocontainers (MWCNTs-EG/AgNPs) were subjected to XRD analysis equipped with Cu Kα radiation over 2θ from 20°–80°, operated at a voltage of 40 kV and a current of 30 mA.

### 2.6.4. Adhesion test

A pull-off adhesion tester of model-DeFelsko Corporation, USA was utilised to determine the adhesion strength of coated mild steel of dimension (30 mm × 40 mm × 1 mm) for blank epoxy coating and loaded with smart nanocontainers (MWCNTs-EG/AgNPs) according to ASTM D4541. The mild steel dollies in a diameter of 20 mm were utilised as adherents. An Araldite epoxy adhesive with two components, specifically hardener and resin with a glue mix ratio of 1:1 was applied to glue the dollies on the coated mild steel surfaces. Five specimens for each blank and modified epoxy were examined with a view to calculate the average value.

## 2.7. Characterisation of smart powder (MWCNTs-EG/AgNPs)

The surface morphology of MWCNTs was examined using A FESEM (model-Hitachi, SU8020) operated at the accelerating voltage of 2 kV, both before and after loaded with green EG/AgNPs inhibitor. A tiny amount of MWCNTs and MWCNTs-EG/AgNPs powder was glued on cylinder stub using double-sided tape. The powder was scanned, and the images were formed by backscattered electrons. The analyser was further fitted with an EDX spectrophotometer to detect the elemental composition of the MWCNTs before and after loaded with smart inhibitor. The thermogravimetry analyser (TGA Q 500) was used to record TGA thermogram of the smart nanocontainers. The smart powder was added into ceramic specimen pan, having height of 5 mm and diameter of 6 mm. Finally, the smart powder was subjected to heat treatment in the range of 30 °C to 1000 °C at the heating rate of 10 °C/min.

## 2.8. Characterisation of EG/AgNPs inhibitor

The crystalline structure of the green EG/AgNPs inhibitor was examined using XRD analysis (Rigaku, SmartLab 3 kW) that used Cu Kα radiation in the angular range of 2θ from (20–90)°, operated at a voltage of 40 kV and a current of 30 mA. TEM (Hitachi HT 7700, BIO-TEM) imaging was performed to determine the shape and size the synthesized nanoparticles. A drop of nanoparticle green inhibitor was located on a carbon-coated copper grid and screened at 120 kV - an operating voltage. The EDX spectra were captured to confirm the existence of AgNPs and other organic elements that constitute the green inhibitor extract and that are also responsible for corrosion inhibition.

## 3. Results and discussion

### 3.1. Characteristics of MWCNTs-EG/AgNPs

#### 3.1.1. FESEM images and EDX spectra

Figure 1 displays the FESEM images of MWCNTs powder without (Fig. 1(a)) and with (Fig. 1(b)) EG/AgNPs inhibitor loaded. The diameters of MWCNTs and MWCNTs-EG/AgNPs were different, where green nanoparticles inhibitors were primarily located in the nanotubes themselves. These caused a mean increase in tubes diameter from 12.7 nm to 42.7 nm, indicating that such inhibitor was successfully loaded inside the carbon nanotubes. The swelling of MWCNTs due to loading with EG/AGNPs inhibitor was in agreement with earlier literature [92,93]. The shared characteristic of the FESEM micrograph is the accumulation of the nanotubes (Fig. 1(b)) as an artefact of powerful surface tension forces between the nanotubes and the solvent during the acetone evaporation phase of the analytical procedure.

Table 3 depicts the EDX spectra of MWCNTs powder without and with EG/AgNPs inhibitor loaded. The appropriate elements were detected on the surface of MWCNTs with C (98.7%). However, the percentage of C was reduced to 82.7% due to the inclusion of green EG/AgNPs inhibitor into MWCNTs. This observation authenticated the existence of EG/AgNPs inhibitor in the MWCNTs.

#### 3.1.2. TGA curves

Figure 2 presents the TGA curve of the MWCNTs and smart nanocontainers MWCNTs-EG/AgNPs. The EG/AgNPs loaded MWCNTs was found to be thermally stable. The TGA curves indicated the extent to which the corrosion inhibitor was grafted in MWCNTs-EG/AgNPs. A decrease in the smart nanocontainers (MWCNTs-EG/AgNPs) weight

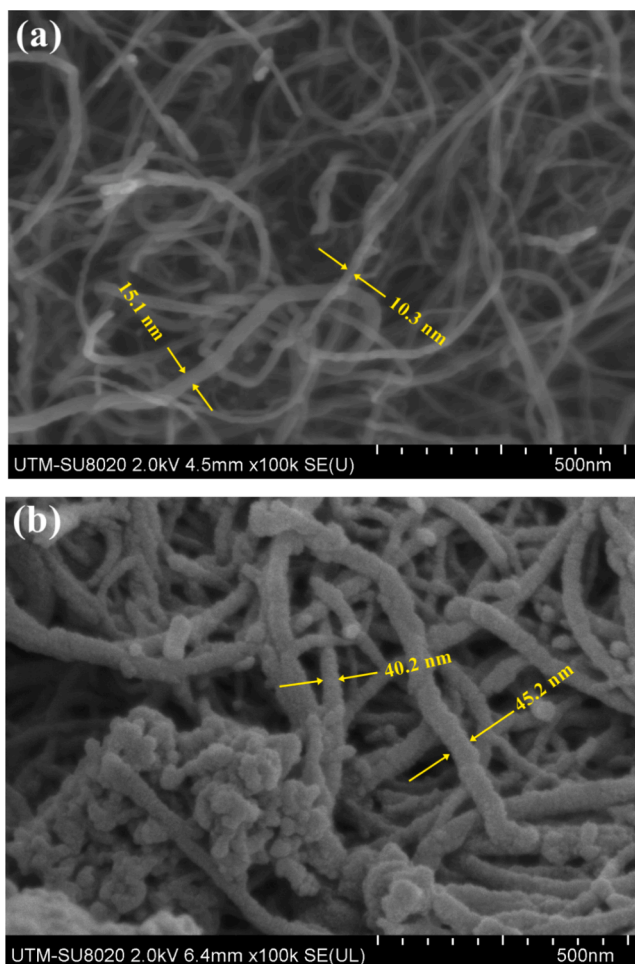


Fig. 1. MWCNTs powder (a) without and (b) with green nanoparticles inhibitor loaded. (For interpretation of the references to colour in this figure legend, the reader is referred to the web version of this article.)

Table 3

EDX elements of MWCNTs with and without EG/AgNPs.

Specimen	Composition (%)		
	O	C	Ag
MWCNTs	1.3	98.7	0.0
MWCNTs-EG/AgNPs	4.0	82.7	13.3

with increasing temperature was observed, revealing three phases of weight loss. The first phase was in the range of 46–180 °C where 0.89 wt % weight losses were observed, which was attributed to the evaporative loss of residual moisture. The second phase of weight loss was appeared between 185 and 500 °C, where 14.58 wt% losses were ascribed to the evaporative release of organic dopant. Lastly, when the temperature was higher than 600 °C, the weight loss was 2.54 wt%, which was approved to the mass loss of different substances. The presence and interaction between MWCNTs and EG/AgNPs inhibitor resulted in a reduced weight loss over these temperature ranges. This is validated the existence of EG/AgNPs inhibitor in MWCNTs and subsequent contribution to assist the coating for withstanding high temperatures.

### 3.2. Properties of AgNPs

Figure 3 shows the XRD pattern of AgNPs, which comprised of four significant diffraction peaks located at  $2\theta$  values of 37.7°, 43.9°, 64.3° and 76.6° indexed to the crystalline lattice planes of (111), (200),

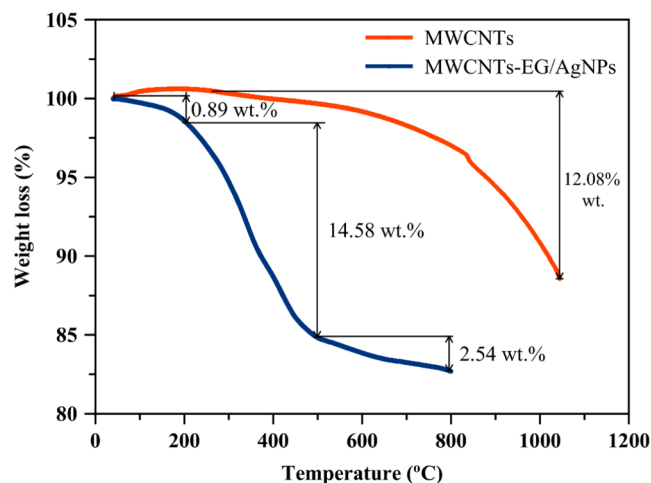


Fig. 2. TGA curve of MWCNTs and smart MWCNTs-EG/AgNPs nanocontainers.

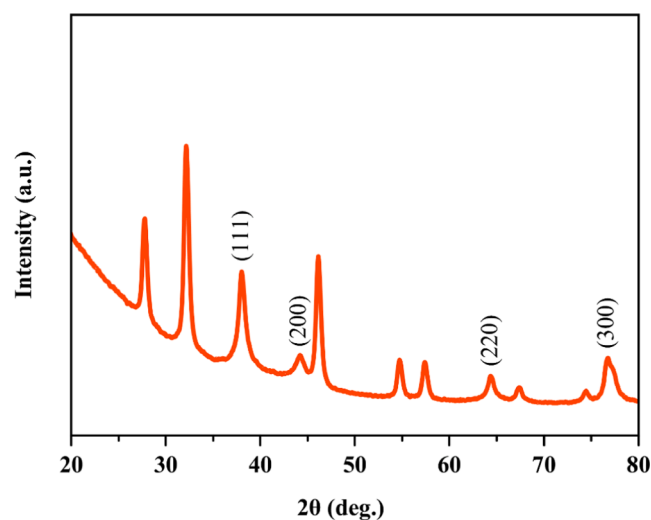


Fig. 3. XRD patterns of the synthesized AgNPs within *Elaeis guineensis* extract.

(220) and (311) of the face centred cubic (fcc) structure of nanoAg. While the other diffraction peaks located at  $2\theta$  values of 27.7°, 32.2°, 46.1°, 54.8°, 57.5°, 67.4° and 74.4° indicated the presence of Tin Telluride (Sn Te) from the inhibitor. AgNPs prepared within *Elaeis guineensis* extract did not reveal any morphological changes. The existence of these peaks verified the orthorhombic crystals structure of nanoAg [94].

Figure 4 depicts the TEM images of green EG/AgNPs inhibitor. The majority of the nanoparticles were spherical with non-agglomerated distributions. Figure 5 illustrates the particles size distribution of EG/AgNPs were ranged within 7.79 nm–30.02 nm in accordance with TEM image (Fig. 4). However, the peak value of EG/AgNPs distribution was found as 13.35 nm. The EDX spectra (Fig. 6) detected the strong silver signal together with C, O and other elements that might be present in *Elaeis guineensis* biomolecules and was bounded to the surface of the AgNPs. However, the presence of heavy metals like Pb (1.8%) might be detected from the plant extract sources which were in-taken from the soil [95–97].

### 3.3. Potentiodynamic polarisation (Tafel) parameters

The potentiodynamic polarisation curves of mild steel in the absence and presence of 5% EG/AgNPs extracts, as well as mild steel coated with blank and 5% MWCNTs-EG/AgNPs modified epoxy are displayed in

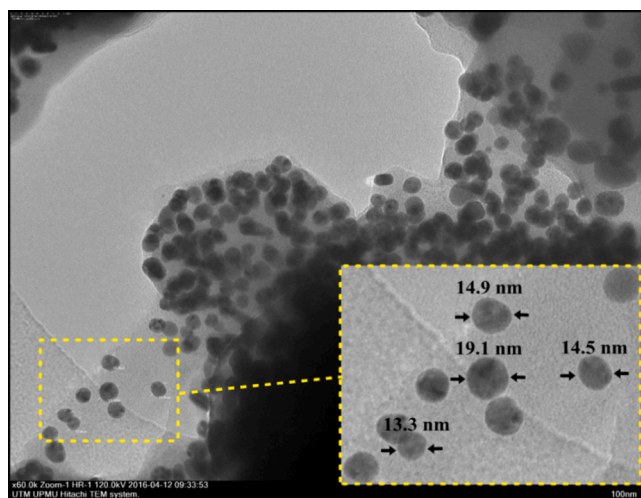


Fig. 4. TEM images of green EG/AgNPs inhibitor. (For interpretation of the references to colour in this figure legend, the reader is referred to the web version of this article.)

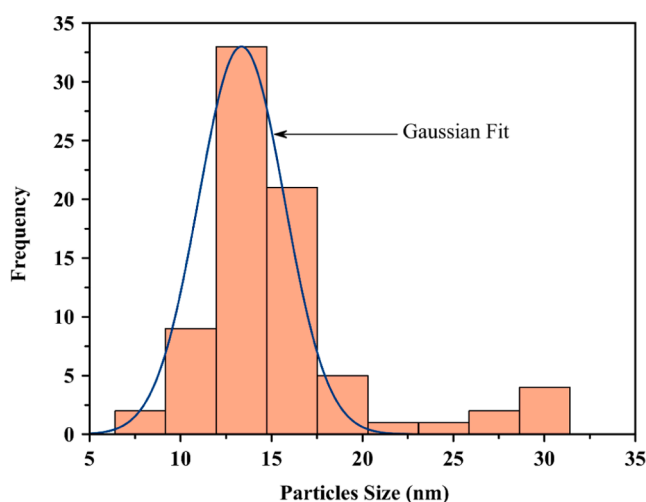


Fig. 5. Particles size distribution of EG/AgNPs in accordance with TEM image together with Gaussian fit.

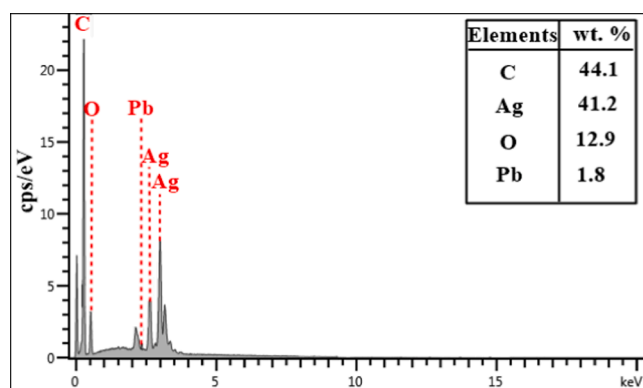


Fig. 6. EDX spectra of EG/AgNPs inhibitor extract.

Fig. 7. The corrosion response of the mild steel in the presence and absence of EG/AgNPs inhibitor alone and with MWCNTs-EG/AgNPs coating was examined via potentiodynamic polarisation measurement after immersing the mild steel in seawater at room temperature for 7, 21,

and 42 days. Polarisation parameters including corrosion potential ( $E_{\text{corr}}$ ), corrosion current density ( $i_{\text{corr}}$ ), anodic ( $b_a$ ) and cathodic ( $b_c$ ) Tafel slopes were derived from the polarisation curves via Tafel region extrapolation as depicted in Fig. 7. Table 4 enlists the achieved potentiodynamic polarisation parameters of mild steel.

The inhibition efficiency of EG/AgNPs extract rises in a concurrent way with immersion time, reaching at the highest value of 93.59% following 42 days of exposure to seawater as shown in Table 4. Nevertheless, it should be noted that the corrosion rate with EG/AgNPs present fell to 0.204 mm/year when compared against 3.174 mm/year, namely, the corrosion rate without EG/AgNPs. In view of this, it is evident that EG/AgNPs extract plays a strong inhibitory role for the corrosion of mild steel in the context of a seawater solution. It should also be noted that the EG/AgNPs inhibitor's cathodic Tafel slope ( $b_c$ ) and anodic Tafel slope ( $b_a$ ) displayed change over time as depicted in Fig. 7 (b) and Table 4. Thus, it is possible to conclude that the inhibitor molecules impacted the pair of reactions and adsorbed on the mild steel surface, which itself occurred by blocking the active sites situated on the surface, thereby inhibiting the corrosion reaction. Furthermore,  $E_{\text{corr}}$  values indicate positive variance with the availability of an inhibitor, especially when compared to blank mild steel. Hence, this indicates the anodic dissolution of mild steel, as well as the cathodic reduction of hydrogen ion depression, which occurs via adsorption of EG/AgNPs extract onto anodic and cathodic surface sites. The implication is that EG/AgNPs compounds function as mixed type inhibitors.

Mild steel with blank epoxy coating (Fig. 7(c) and Table 4) demonstrated a value of  $E_{\text{corr}} = -0.250$  V after 7-day which was increased to  $-0.379$  V after 42 days exposure to seawater. In contrast, the current density for blank coated coupons in the scratched area was increased from  $1.412 \mu\text{A}\cdot\text{cm}^{-2}$  to  $2.286 \mu\text{A}\cdot\text{cm}^{-2}$  whilst the corrosion rate was increased from  $0.6465$  mm/y (at 7-day exposure) to  $1.0465$  mm/y (at 42 days exposure), indicating the significance of absence of surface protection at the scratched area in combination with exposure to chloride ions mediated aqueous solution. The constitutions of both the cathodic and anodic portions of the polarisation curve produced by the blank coating is entirely modified by the addition of 5% MWCNTs-EG/AgNPs as depicted in Fig. 7(d).

The shift in polarisation curves towards a more noble potential of  $-0.034$  V accompanied by lower current density of  $0.075 \mu\text{A}\cdot\text{cm}^{-2}$  was observed due to the inclusion of MWCNTs-EG/AgNPs containers. In addition, the week 1 analysis of corrosion current ( $i_{\text{corr}}$ ) values showed reduction from  $1.412$  (blank coatings) to  $1.002 \mu\text{A}\cdot\text{cm}^{-2}$  (self-healing coatings); correspondingly  $E_{\text{corr}}$  values as well-found shift in cathodic direction from  $0.250$  to  $0.365$  V. This evident that under electrochemical cell stimulation, steel corrosion initiates on week 1 itself; which subsequently releases the self-healing coating's inhibitors (MWCNTs-EG/AgNPs) and controls corrosion by suppress cathodic reaction. Till day 21 analysis, similar trend was observed for both blank coating and self-healing coating (i.e.)  $E_{\text{corr}}$  shifted in cathodic side and correspondingly reduces corrosion current ( $i_{\text{corr}}$ ) values. These observations evident that epoxy coating is predominantly controls corrosion in either case of blank/self-healing coatings while the MWCNTs-EG/AgNPs enhance the protection ability in later case. This may because, the oxygen transfer from corrosive solution to the metal/solution interface will strongly affect the rate of oxygen reduction according to,



The above can be inferred that the adsorbed coating layer behaves as a cathodic inhibitor by retarding the  $\text{O}_2$  diffusion to the cathodic sites of the metal surface. This indicates that epoxy coatings inhibit corrosion process of the mild steel predominantly through cathodic mode and MWCNTs-EG/AgNPs enhances the corrosion protection of self-healing coating. The 42nd day results for blank coating followed the same trend of earlier (7th and 21st day) observations; while self-healing coating shown deep anodic shift from  $-0.531$  V to  $-0.034$  V and

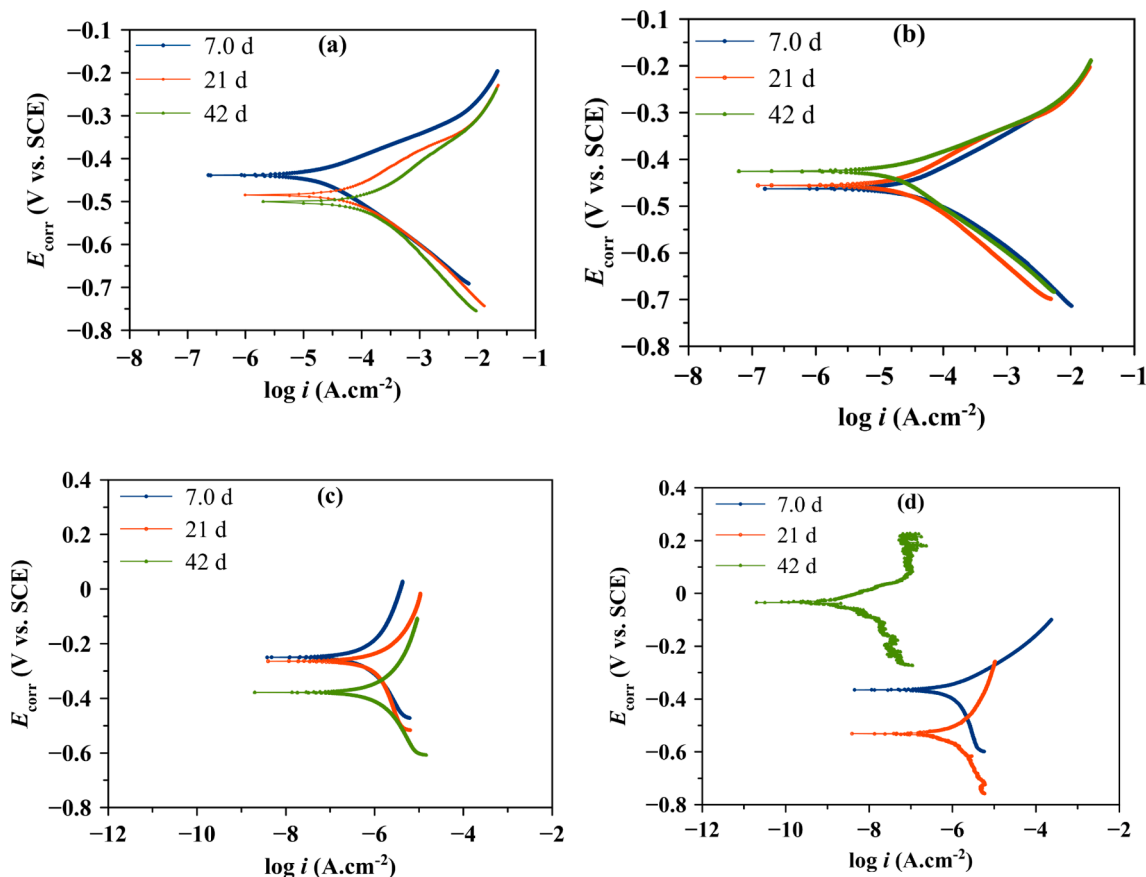


Fig. 7. Potentiodynamic polarisation curves of mild steel surface after exposure to seawater with (a) bare, (b) EG/AgNPs inhibitor, (c) blank coating and (d) MWCNTs-EG/AgNPs modified epoxy coating.

Table 4  
Potentiodynamic polarisation parameters of mild steel surface, bare and with EG/AgNPs inhibitor, blank and MWCNTs-EG/AgNPs modified epoxy coating.

Specimen	Exposure time (day)	Tafel					Corrosion rate (mm/y)
		$-E_{corr}(V)$	$i_{corr}(\mu A.cm^{-2})$	$b_a(V/dec)$	$-b_c(V/dec)$	IE%	
Bare mild steel	7.0	0.438	90.072	0.067	0.101	-	1.028
	21	0.485	113.214	0.087	0.110	-	1.249
	42	0.501	157.591	0.106	0.142	-	3.174
EG/AgNPs	7.0	0.462	35.728	0.089	0.098	60.33	0.408
	21	0.455	26.344	0.081	0.097	76.73	0.291
	42	0.425	10.109	0.083	0.088	93.59	0.204
Blank coating	7.0	0.250	1.412	0.245	0.224	-	0.6465
	21	0.264	2.262	0.119	0.687	-	1.0353
	42	0.379	2.286	1.180	5.680	-	1.0465
Self-healing coating	7.0	0.365	1.002	0.867	0.632	29.04	0.0081
	21	0.531	0.687	0.395	0.246	69.63	0.0056
	42	0.034	0.075	0.613	0.581	96.72	0.0009

correspondingly lowered  $i_{corr}$  values from 0.687 to 0.075  $\mu A.cm^{-2}$ . This clearly evident that during long exposure period, embedded corrosion inhibitor (MWCNTs-EG/AgNPs) released more which may leads the protection action over epoxy coating. These results are in agreement with the literature [98,99].

The observed corrosion reduction (enhanced corrosion resistance) was attributed to the effect of a re-passivation process occurred from the self-healing properties of the conversion coating [100–102]. It indicated that blocking of areas of the mild steel surface is the mechanism by which corrosion protection was afforded by the coating which in turn caused minimal oxygen reduction and metal dissolution within the pores of the coating layers. Furthermore, the blank coating augmented the

values of  $b_a$  and  $b_c$  to 1.180 V/dec and 5.680 V/dec, respectively following 42 days of exposure, whilst the  $b_a$  and  $b_c$  for the MWCNTs-EG/AgNPs coating was correspondingly decreased to 0.613 V/dec and 0.581 V/dec for the same exposure period. It was asserted that the MWCNTs-EG/AgNPs coating could minimise the mild steel corrosion rate via blocking of both anodic and cathodic sites. Furthermore, the coating material comprising of 5% of MWCNTs-EG/AgNPs exhibited the lowest corrosion rate of 0.0009 mm/y than the one with blank coating (1.0465 mm/y) and highest inhibition efficiency reached to 96.72%. The efficacy of smart coating was in good agreement with the results achieved by the literature reported for mild steel's smart coating development using epoxy nanocomposite coatings blended with

corrosion inhibitor functionalized nanoparticles, and hybrid nano-coating of polyvinyl alcohol and Titania against NaCl solution [103,104] respectively. It was concluded that the self-healing agent (EG/AgNPs) offered a significant barrier against corrosive species and thus promoted the overall mild steel corrosion resistance.

### 3.4. Electrochemical impedance spectra

The corrosion behaviour of epoxy coated MS in a seawater solution was examined by EIS method, in presence and absence of 5% EG/AgNPs at 7, 21, and 42 days. The open circuit potential (OCP) was measured before the electrochemical analysis and the respective results were depicted in Fig. 8. The stable OCP was obtained (approximately after 25 min) which evident the attainment of steady state after 30 min time. Fig. 9 depicts the electrical equivalent Randles circuit for plain and coated mild steel, where  $R_s$  is the solution resistance,  $R_f$  is the resistance of portative film over mild steel surface,  $Q_{dl}$  and  $Q_f$  are the constant phase angle elements (CPE), representing double-layer capacitance  $C_{dl}$  and, film capacitance  $C_f$ , respectively.  $R_{ct}$  is the charge-transfer resistance for mild steel. Various equivalent circuits were generated and fitted against the experimental impedance values, while the circuit that having lowest fitting error was selected.

Regarding the use of EIS in the context of plain mild steel in seawater, Nyquist plots were gathered, and these are outlined for the presence and absence of 5% EG/AgNPs inhibitor in Fig. 10 (a and b) respectively. Based on the impedance spectra, it is clear that the increase of the semicircle diameter is directly and proportionally related to the exposure time of mild steel when the EG/AgNPs inhibitor is present. With the observation of the semi-circular shape in the case of blank mild steel and with EG/AgNPs present, it was shown that the corrosion mechanism was identical regardless of the absence or presence of EG/AgNPs inhibitor [105]. Several factors can be attributed to the depressed semicircle depicted in the Nyquist plots regarding the ideal case, including frequency dispersion, the adsorption of inhibitive compounds,

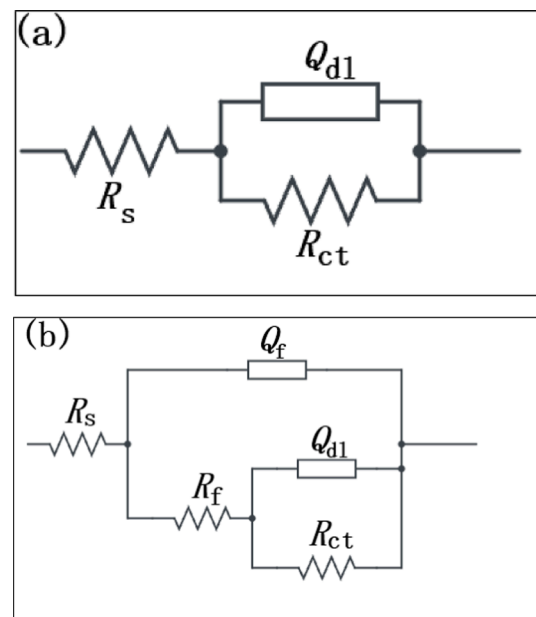


Fig. 9. The electrical equivalent Randles circuit for (a) bare mild steel and (b) coated mild steel.

the surface's inhomogeneity levels, and polycrystallinity [106]. As shown in Fig. 10(a), the reduction of  $-Z''$  at high frequencies for mild steel with the absent of EG/AgNPs inhibitor can be linked to the adsorption of several aggressive species, including  $Cl^-$  ions. In contrast, the higher diameter of capacitive loops (Fig. 10(b)) is indicative of an increase in charge transfer resistance, as well as a fall in corrosion current density. As a consequence of this, addition of 5% EG/AgNPs protects mild steel surface and conversely suppress the corrosion rate.

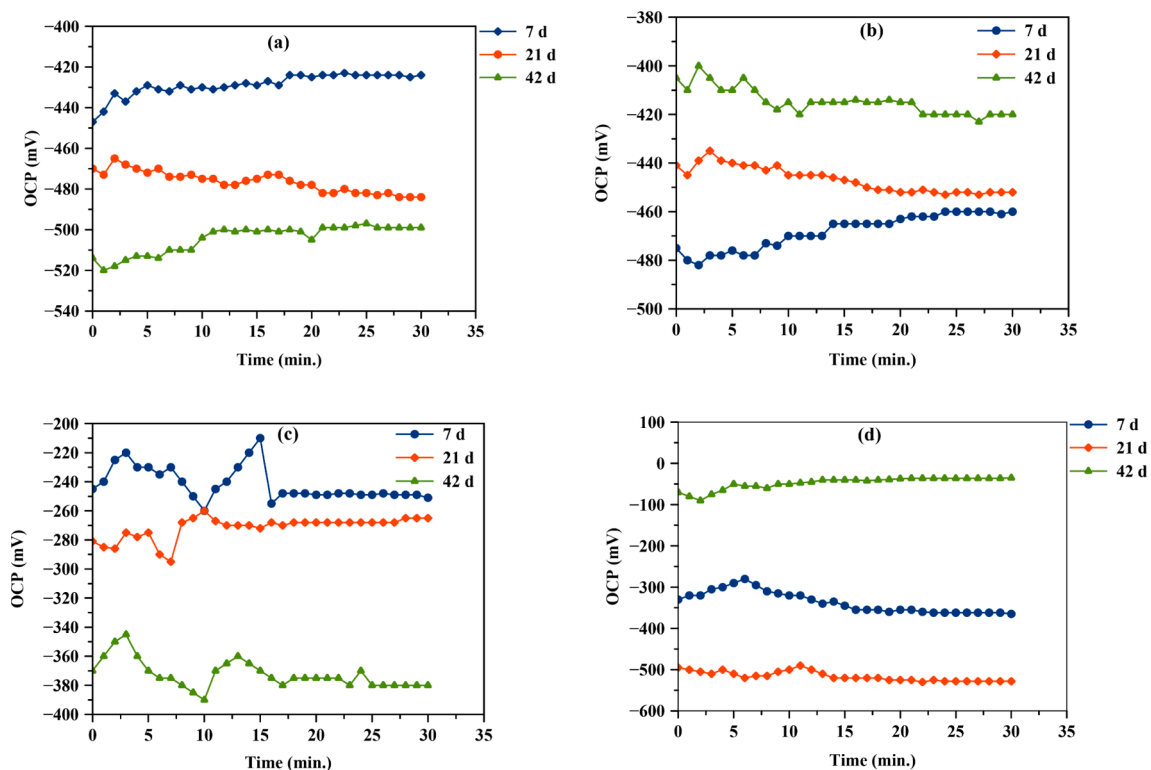


Fig. 8. Open circuit potential of mild steel surface immersed in seawater with (a) bare, (b) EG/AgNPs, (c) blank coating and (d) MWCNTs-EG/AgNPs modified epoxy coating.

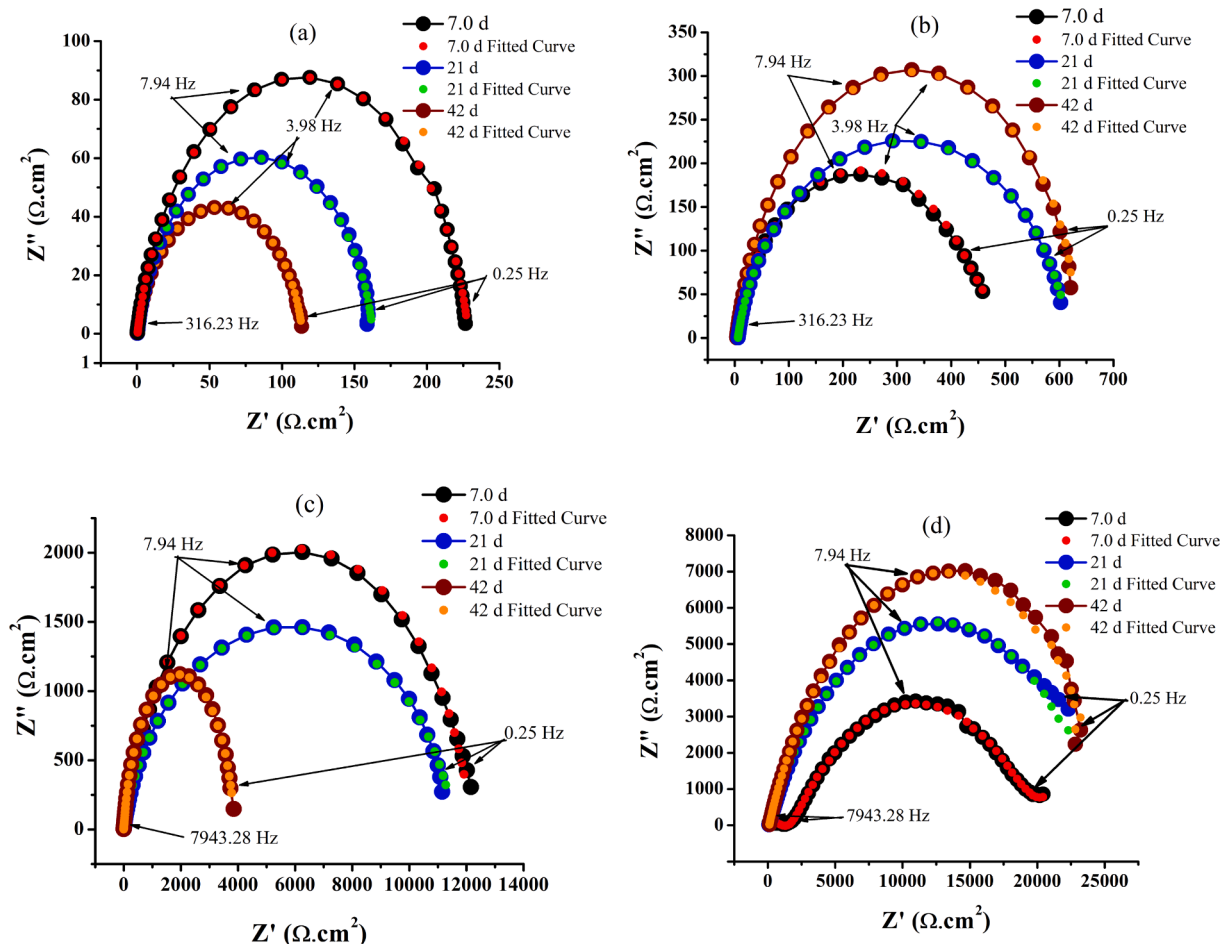


Fig. 10. Nyquist diagram of mild steel surface with (a) bare, (b) EG/AgNPs, (c) blank coating and (d) MWCNTs-EG/AgNPs modified epoxy coating.

The highest IE (%) was observed at 42 days (Table 5), with a percentage of 93.67%. Based on these outcomes, it is clear that charge transfer resistance ( $R_{ct}$ ) rises considerably in line with the length of time exposed to the inhibitor. The highest value for impedance was identified for EG/AgNPs extract ( $6.83 \times 10^2 \Omega.cm^2$ ), and this was paired with the tendency to fall for the double-layer capacitance  $C_{dl}$  to  $16.2 \mu F.cm^{-2}$  compared with  $97.1 \mu F.cm^{-2}$  in the absence of EG/AgNPs extract. This behaviour is attributed with increase in the protective layer's thickness at the electrode surface, which promotes mild steel corrosion resistance. The rise in  $R_{ct}$  values is linked to the development of the protective layer at the metal/solution interface. In view of these observations, it is possible to conclude that the inhibitor extract operates via adsorption at

the surface of the metal, which blocks charge transfer across the metal/solution interface, thus inhibiting corrosion. This is supported by the decrease in  $C_{dl}$  values, paired with the attendant rise in inhibition efficiency. The literature evidence shows that *Elaeis guineensis* include alkaloids, terpenoids, saponins, flavonoids, tannins, phenolic compounds, carbohydrate, and coumarins [107], and when these compounds are adsorbed via the aromatic ring, as well as the heteroatoms of nitrogen and oxygen upon the mild steel surface, this can hinder against the ingress of corrosive ions into the solution. This is because the compounds establish a barrier associated with mass and charge transfer.

Further, the self-healing properties of the MWCNTs-EG/AgNPs coating were evaluated using EIS measurement, where the coated mild

Table 5

EIS parameters of mild steel surface, bare and with EG/AgNPs inhibitor, blank and MWCNTs-EG/AgNPs modified epoxy coating.

Specimen	Exposure time (day)	$R_s(\Omega.cm^2)$	$R_f(\Omega.cm^2)$	$R_{ct}(\Omega.cm^2)$	$C_f(\mu F.cm^{-2})$	$C_{dl}(\mu F.cm^{-2})$	IE %
Bare mild steel	7.0	4.88	-	7.49	-	59.4	-
	21	4.58	-	5.86	-	66.3	-
	42	5.27	-	4.32	-	97.1	-
EG/AgNPs	7.0	4.99	-	$1.90 \times 10^2$	-	28.6	60.47
	21	4.86	-	$2.52 \times 10^2$	-	22.9	76.72
	42	4.73	-	$6.83 \times 10^2$	-	16.2	93.67
Blank coating	7.0	$2.61 \times 10^2$	54.813	$9.88 \times 10^3$	$8.67 \times 10^{-1}$	$1.52 \times 10^{-1}$	-
	21	$1.57 \times 10^2$	23.550	$4.51 \times 10^3$	$32.98 \times 10^{-1}$	$4.74 \times 10^{-1}$	-
	42	$2.68 \times 10^2$	19.841	$1.11 \times 10^3$	$47.35 \times 10^{-1}$	$6.34 \times 10^{-1}$	-
Self-healing coating	7.0	$1.68 \times 10^2$	450.2	$2.25 \times 10^4$	$3.12 \times 10^{-1}$	$2.01 \times 10^{-3}$	56.09
	21	$2.57 \times 10^3$	1031.8	$4.69 \times 10^4$	$2.39 \times 10^{-1}$	$1.05 \times 10^{-3}$	90.38
	42	$1.61 \times 10^4$	1897.5	$8.25 \times 10^5$	$0.86 \times 10^{-1}$	$1.59 \times 10^{-4}$	97.87

steel was immersed in seawater for different duration. The electrochemical behaviour of mild steel specimens and the impact of MWCNTs-EG/AgNPs on the barrier properties mild steel were determined. EIS measurements were performed for the scratched area of both the blank epoxy specimen and epoxy specimen loaded with MWCNTs-EG/AgNPs.

Figure 10 also illustrates the Nyquist plot of the seawater exposed mild steel specimen with blank epoxy coating (Fig. 10(c)) and the one included to smart MWCNTs-EG/AgNPs nanocontainers (Fig. 10(d)). The polarisation resistance of the test specimens was characterised by the diameter of the capacitive loops in the Nyquist plot, where bigger capacitive loop signified lower corrosion rate [108]. Table 5 presents the values of EIS parameters of mild steel for blank epoxy coating and MWCNTs-EG/AgNPs modified epoxy coating. The resistance of portative film and the charge transfer resistance of the blank coating were  $54.813 \Omega \cdot \text{cm}^2$  and  $9.88 \times 10^3 \Omega \cdot \text{cm}^2$  after 7 days of seawater immersion. However, for long duration immersion the blank coating portative film resistance values and the charge transfer resistance were gradually reduce. For 42 days of seawater immersion, the values of the blank coating including portative film resistance and the charge transfer resistance were decrease to  $19.841 \Omega \cdot \text{cm}^2$  and  $1.11 \times 10^3 \Omega \cdot \text{cm}^2$ , respectively. The reduction of impedance values with increasing the period of exposure is obviously indicated that the barrier properties of the film are decreased due to the dispersion of electrolytes into the coating matrix. Conversely, the value of film capacitance  $C_f$  and the double-layer capacitance of the blank coating were increased from  $0.867 \mu\text{F} \cdot \text{cm}^{-2}$  to  $4.735 \mu\text{F} \cdot \text{cm}^{-2}$  and  $0.152 \mu\text{F} \cdot \text{cm}^{-2}$  to  $0.634 \mu\text{F} \cdot \text{cm}^{-2}$ , respectively during the studied period. The observed reduction in the portative film resistance and enhancement in the capacitance for the blank coating over the studied period was correlated to the corrosion properties of epoxy. On the contrary, the incorporation of MWCNTs-EG/AgNPs was attributed to the strengthening of the coating throughout decreasing its porosity. Hence, the portative film resistance of MWCNTs-EG/AgNPs coating surface was increased from  $450.2 \Omega \cdot \text{cm}^2$  (7 days) to  $1897.5 \Omega \cdot \text{cm}^2$  (42 days) of submersion in seawater. Furthermore, the improvement of the barrier properties of the modified coating can be related to the formation of a protective film due to the adsorption of inhibitor molecules upon the mild steel surfaces [109]. The remarkable enhancement in the charge transfer resistance values for the MWCNTs-EG/AgNPs modified epoxy coating (Fig. 10(d)) was attributed to the anti-corrosive impact of green EG/AgNPs inhibitor. Besides, the double-layer capacitance  $C_{dl}$  and, film capacitance  $C_f$  were correspondingly reduced from  $2.01 \times 10^{-3} \mu\text{F} \cdot \text{cm}^{-2}$  to  $1.59 \times 10^{-4} \mu\text{F} \cdot \text{cm}^{-2}$  and  $3.12 \times 10^{-1}$  to  $0.86 \times 10^{-1}$ , respectively over the same period of immersion. The increasing of coating charge resistance from  $2.25 \times 10^4 \Omega \cdot \text{cm}^2$  to  $8.25 \times 10^5 \Omega \cdot \text{cm}^2$  and reducing the coating capacitances under the same conditions can be attributed to the increasing the inhibition efficiency of modified coating to 97.87%. The results of inhibition efficiency are comparable with the literature that hindered the corrosion of mild steel by using a water-based hybrid organo-silane film combined with non-toxic organic-benzimidazole/ inorganic-praseodymium inhibitors [110], and by the development of active barrier, affected the hybrid chitosan/silica composite epoxy-based coating [111] against NaCl solutions. Also, the coating that exhibited low film capacitance  $C_f$  ( $0.86 \times 10^{-1} \mu\text{F} \cdot \text{cm}^{-2}$ ) for modified coating compared to the high  $C_f$  ( $47.35 \times 10^{-1} \mu\text{F} \cdot \text{cm}^{-2}$ ) for the epoxy coating after 42 days of exposure, which indicates a good anti-corrosion performance over the mild steel surface. While the rise of  $C_f$  values with exposure time as listed in Table 5, demonstrating the continued deterioration of the coating in the aggressive solution [112]. It's worthy to note that, the significant deviation between the measured data and the fitted curves at high frequencies in the Nyquist plots as depicted in Fig. 10 (a, c, and d) at 7 and 21 days is related to other origins frequency dispersion such as the adsorption of  $(\text{Cl}^-)$  ions [113]. This achieved high resistance and low capacitance of the MWCNTs-EG/AgNPs coating was ascribed to the impact of green EG/AgNPs inhibitor that could produce a protective oxide film with self-healing properties on the mild steel surface. Present

findings also confirmed that the embedment of green nanoparticles into the organic coating could produce significant benefits with respect to the long-term barrier protective properties.

Figure 11 depicts EIS Bode plots, which characterised the time constant within the high frequency range associated with the protective barrier properties of the coatings. The magnitude of the capacitive slope within this high frequency range was found to be identical for all specimens following 7 days of immersion in seawater. This was expected since the coatings have similar thickness. Additionally, the bigger  $|Z|$  (low-frequency impedance modulus), shows a good corrosion prevention performance [114]. Conversely, blank coating (Fig. 11(a)) revealed a significant decrease in the frequency region  $|Z|$  at 42 days, whilst the self-healing coating exhibited high frequency range at 42 days of immersion in seawater (Fig. 11(b)). These results demonstrate that the composite coating improves the inhibition performance of mild steel against corrosion in seawater solution.

Figure 11 shows the phase angle plots of mild steel with blank and MWCNTs-EG/AgNPs inhibitor modified epoxy coating. The blank coating exhibited a considerable reduction in the phase angle over the high frequency region combined with a reduction in the impedance modulus (Fig. 11(a)). Meanwhile, the self-healing coating revealed an increase in the phase angle from 7 days to 42 days of immersion in seawater (Fig. 11(b)). The observed notable deterioration of the protection film on mild steel for blank coating was due to the exposure of seawater. This finding takes consideration of the massive defects developed in the blank coating following 42 days of seawater

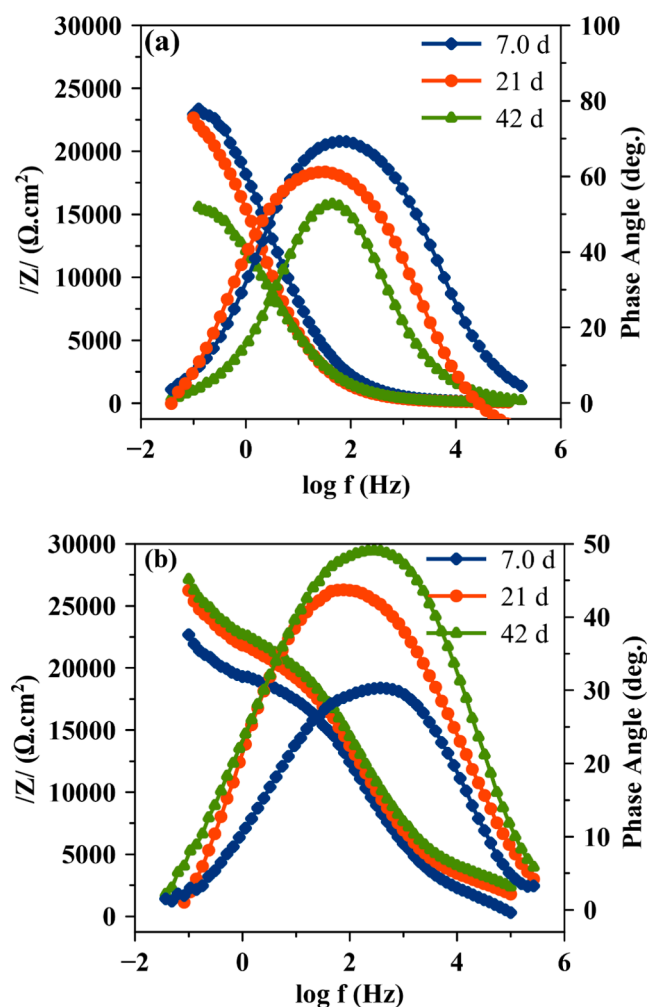


Fig. 11. Bode plots for mild steel surface with (a) blank coating and (b) MWCNTs-EG/AgNPs modified epoxy coating.

immersion.

### 3.5. SEM images and EDX spectra

The surface morphological features of mild steel coupons were examined using SEM after immersion in seawater for a 42-day period. Initially, SEM screening was carried over mild steel immersed in corrosive medium in absence (Fig. 12(a))/presence (Fig. 12(b)) of 5% EG/AgNPs extract. In the absence of the inhibitor, the findings indicate a severe deterioration of the mild steel surface, which stems from metal dissolution. Fig. 12(a) indicates that the surface has become rough after immersion in seawater, accompanied by an obvious net of cracks. The findings indicate that this deterioration was attenuated considerably when the EG/AgNPs extract was present. Fig. 12(b), clearly indicated that the corrosion rate was reduced owing to the adsorption of the inhibitor molecules on the mild steel surface, thereby formation of a protective layer between the mild steel and the corrosive environment.

Further, SEM analysis was carried out for mild steel with epoxy coating. Fig. 12 displays the SEM micrographs of scratched mild steel prior to the immersion in seawater with blank coating (Fig. 12(c)), and after immersing in seawater with blank coating (Fig. 12(d)) and MWCNTs-EG/AgNPs inhibitor modified epoxy coating (Fig. 12(e)). The self-healing properties of different aqueous epoxy coatings were inspected by introducing two identical artificial defects onto the surface of the blank coating and also the test coating loaded by 5% of MWCNTs-EG/AgNPs. The defects produced by the blade were clearly seen (Fig. 12(c)), which touched the metal surface to create wide scratch ranged up to 430.2 μm. These scratches appeared relatively smooth and levelled prior to the immersion of mild steel in seawater. The entire scratch area of the blank coating (Fig. 12(d)) became highly corroded following submersion in seawater for 42 days, where the damage surrounded by corrosion by-products was evidenced. Furthermore, no change was observed to the width of the scratched region, corrosion by-product precipitates proliferated over scratched area with time.

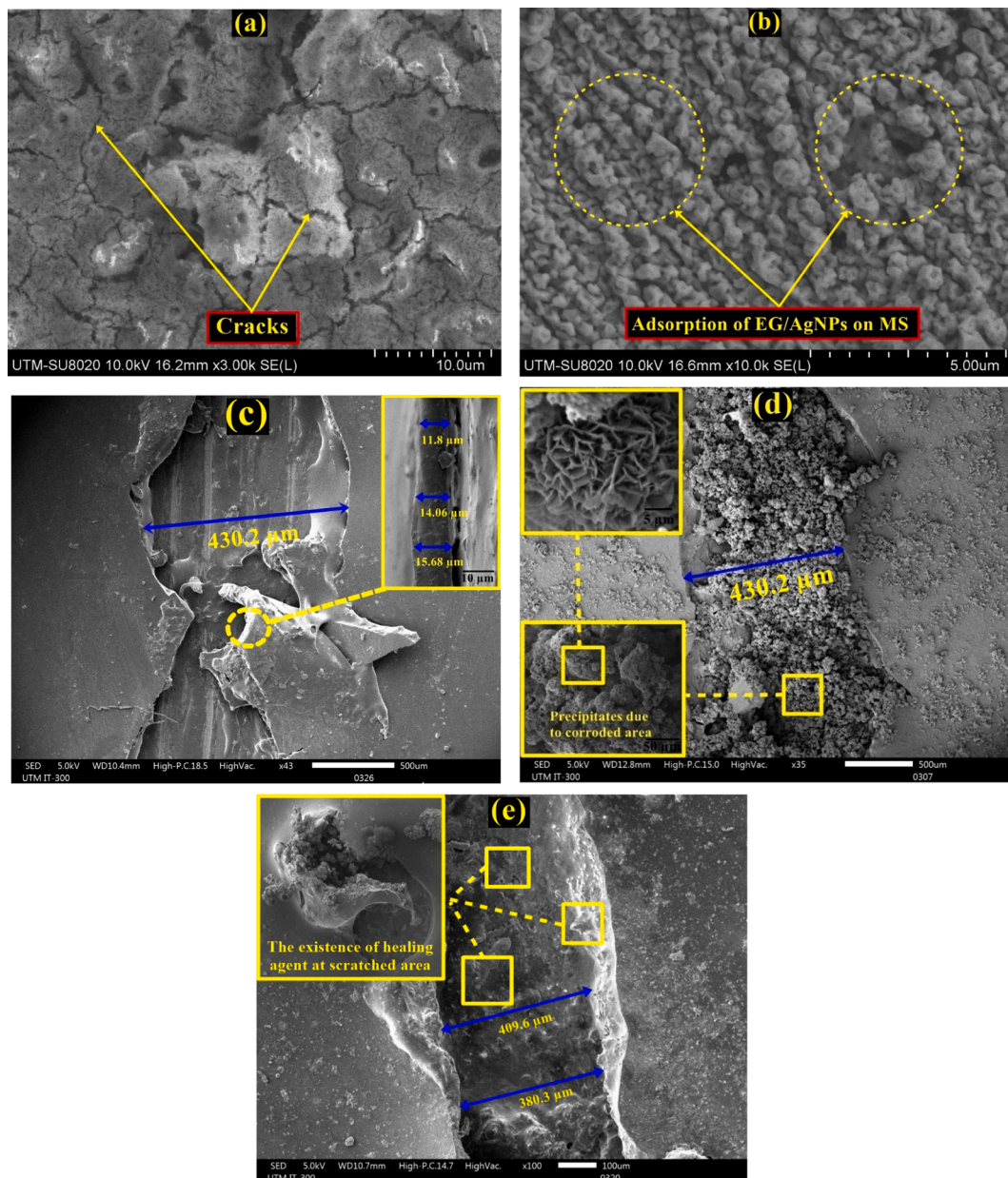


Fig. 12. SEM micrographs of mild steel surface after immersed in seawater (a) bare, (b) EG/AgNPs, (c) scratched mild steel before immersing in seawater and scratched mild steel with immersing in seawater (d) blank coating and (e) modified coating.

The detection of the presence of areas of undercoating corrosion with delamination and blistering of the blank coating, provides further indication of high corrosion activity. Conversely, the smart nanocontainers assisted coating could seal the scratched area within the smart epoxy coating by releasing healing compounds immediately after the creation of the scratch. Subsequently, the scratch width was slowly narrowed to 380.3  $\mu\text{m}$  and then entirely covered with the green nanoparticles inhibitor (Fig. 12(e)). Moreover, no indication of delamination or undercoating corrosion was observed and the similar observations were made earlier as well [115–117]. These could represent an indication that green inhibitor (EG/AgNPs) could dry and seal the defect area by oxidation with atmospheric oxygen. The smart coating with healing layer of 13.85  $\mu\text{m}$  demonstrated pronounced healing, repairing of the surface scratching, and also promoted the lifespan of mild steel in corrosive seawater environments.

To further analyse the protective behaviour of MWCNTs-EG/AgNPs coating against corrosion, the EDX analysis was carried out. Table 6 presents the EDX spectra of mild steel with blank and MWCNTs-EG/AgNPs inhibitor modified epoxy coating. The EDX spectra could clearly detect the chemical elements present in the scratched area after submersion in seawater for 42 days. Table 6 depicts detected elemental traces in mild steel with blank and modified coating. The presence of Fe (21.5%) and O (15.8%) elements on the blank coated mild steel surface was detected, suggesting the production of iron hydroxide and high corrosion activity over the scratched area. Furthermore, the presence of MWCNTs-EG/AgNPs in the coated area exhibited corrosion protection activity over the scratched area, wherein the amount of adsorbed chloride ions ( $\text{Cl}^-$ ) were reduced from 23.4% to 0.9%, and Fe dropped to 1.0%. This clearly verified the self-healing abilities of the MWCNTs-EG/AgNPs incorporated epoxy coating. The O levels were increased to 27.1% for in the presence of MWCNTs-EG/AgNPs coating, which confirmed that the smart EG/AgNPs acted as a good mild steel corrosion inhibitor. The SEM images, EDX spectra strongly supported the EIS and polarisation results.

### 3.6. XRD pattern

Figure 13 presents the X-ray diffraction patterns for the coated mild steel specimens with and without MWCNTs-EG/AgNPs following immersion in seawater for 42 days. As indicated, the peaks at  $2\theta$  values of 23.97°, 46.25° and 52.07° can be assigned to the iron oxides in the form of magnetite ( $\text{Fe}_3\text{O}_4$ ), while the peaks at  $2\theta$  values of 37.58° and 57.73° can be assigned to the oxyhydroxides in the form of lepidocrocite ( $\gamma\text{-FeOOH}$ ). In addition, the peaks at  $2\theta$  values of 43.12° and 58.43° correspond to iron. A number of the lepidocrocite peaks of mild steel coupon with smart (MWCNTs-EG/AgNPs) coating are seen to become weakened or lost following immersion in the presence of MWCNTs-EG/AgNPs, indicating that the smart nanocontainers sealed the scratched area by releasing of EG/AgNPs inhibitor and formed as a barrier to prevent the  $\text{Cl}^-$  ions to reach the mild steel surface and hence further hindering the corrosion process.

### 3.7. Immersion test of Self-Healing coatings

The self-healing capabilities and anticorrosion behaviour of the smart coatings was verified via long-term immersion tests in seawater, where mild steel was coated with blank epoxy and MWCNTs-EG/AgNPs

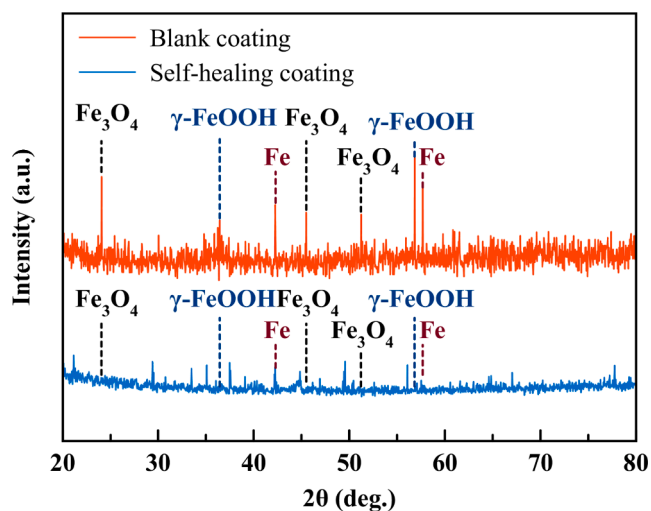


Fig. 13. XRD patterns of scratched mild steel surface with blank and MWCNTs-EG/AgNPs modified epoxy coating.

modified epoxy. Fig. 14 illustrates the time dependent evolution of the artificial scratches on the blank epoxy (Fig. 14(a)) and MWCNTs-EG/AgNPs modified (Fig. 14(b)) epoxy coated mild steel immersed in seawater. Following 42 days of submersion in seawater of the mild steel coupon with the blank epoxy coating, visual inspection indicated significant deterioration of the mild steel coupon and the formation of rusty, brown and weakly adherent corrosion products which proliferated over the scratched area (Fig. 14(a)). Moreover, modified smart coating (MWCNTs-EG/AgNPs) on mild steel surface revealed excellent repair attributes (Fig. 14(b)) with remarkable pronounced self-healing capability of scratch repair. It was established that the scratched region remained smooth and corrosion-free following submersion in seawater for 42 days.

Table 7 provides an overview of the adhesion strength associated with various surface roughness types. Results clearly evidenced for adhesive combined with MWCNTs-EG/AgNPs nanoparticles, adhesion strength was significantly enhanced when comparatively examined against blank epoxy adhesive. In particular, adhesion strength increased from 2.88 MPa to 6.36 MPa. It is worth considering that the even dispersion of nanoparticles can affect the physical and chemical properties of the adhesion for epoxy adhesive. This is because they offer reinforced anchoring, thereby promoting adhesion strength owing to their location in the steel surface asperities [118]. Nevertheless, the rise in AS could also be linked to the nanoparticles' chemical attributes, which could in turn affect the chemical properties of the steel and epoxy adhesive surfaces, thereby giving rise to chemical bonds on each steel-adhesive interface and subsequently promoting adhesion strength. In this case, the probability is that nanoparticles serve as intermedia, the purpose of which is to span the superficial atoms or molecules of steel and epoxy adhesive. The reasonable mechanism was considered that the rough surface could magnify the interaction area for epoxy and steel, with the nanoparticles underpinning the reinforcement of the impact. As such, a greater number of possibilities associated with mechanical interlocking and chemical bonds could emerge. In the context of a smooth surface, the absence of this anchoring mechanism would be the case. Resultantly, for the modified coating with smart nanocontainers,

Table 6

EDX elements of mild steel surface with blank and MWCNTs-EG/AgNPs modified epoxy coating.

Specimen	Composition (%)										
	Fe	C	O	Ca	Mg	Cl	Na	Ag	S	K	Si
Blank coating	21.5	21.8	15.8	0.2	1.7	23.4	14.1	0.0	1.0	0.3	0.2
Modified coating	1.0	60.2	27.1	0.3	0.0	0.9	0.0	10.3	0.0	0.2	0.0

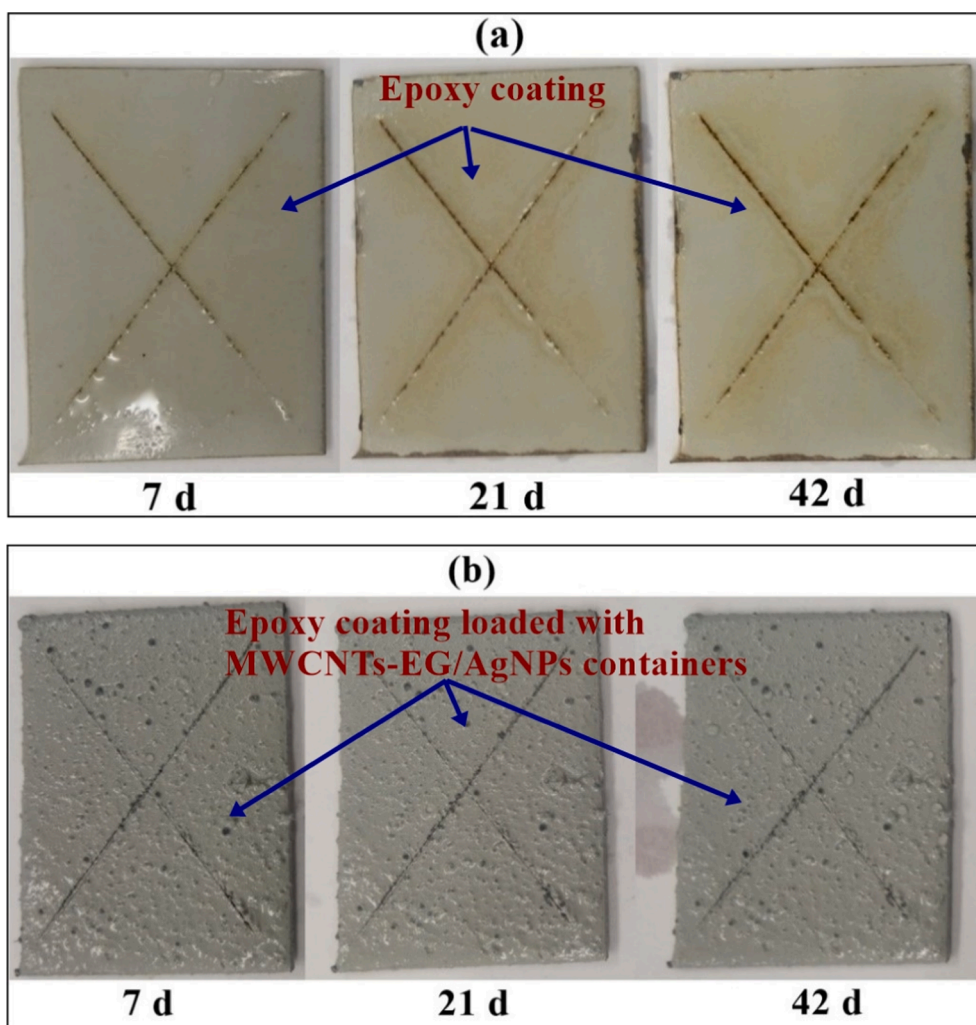


Fig. 14. The time dependent evolution of artificial scratches on coated mild steel surface immersed in seawater (a) epoxy coating, and (b) (smart epoxy coating).

Table 7

The adhesion strength of coated mild steel surface with blank and modified epoxy coating.

Specimen	Pull 1 (MPa)	Pull 2 (MPa)	Pull 3 (MPa)	Pull 4 (MPa)	Pull 5 (MPa)	Average pull value
Blank coating	3.1	2.7	2.8	2.8	3.0	2.88
Modified coating	6.4	6.7	5.9	6.3	6.5	6.36

the steel surface’s adhesion strength was considerably higher than when compared to blank epoxy.

The mild steel coupon with smart (MWCNTs-EG/AgNPs) coating satisfactorily passed the adhesion test, demonstrating that the inhibitor coating adhesion was not influenced due to the exposure of the seawater. Meanwhile, the barrier performance was not yet nearly repaired without releasing the green nanoparticles inhibitor (EG/AgNPs).

### 3.8. Properties of MWCNTs-EG/AgNP (Smart Coating)

#### 3.8.1. AFM images

Figure 15 shows the AFM images of coated mild steel surface with blank epoxy (Fig. 15(a)) and modified epoxy with MWCNTs-EG/AgNPs (Fig. 15(b)) prior to immersing in seawater. The image for the blank

coating illustrated a 700 nm height of mild steel specimen which appeared comparatively smoother with root mean square (RMS) surface roughness of 326.9 nm (Fig. 15(a)). Although both type of coating produced homogeneous surfaces but the MWCNTs-EG/AgNPs modified smart coating mediated surface displayed somewhat roughness with RMS value of 1.246 μm and height of 1.6 μm (Fig. 15(b)). The presence of some large substrate particles was evidenced, which was due to the agglomeration of smaller nanotubular particles.

#### 3.8.2. FESEM images

Figure 16 shows the high-resolution SEM micrograph of smart materials coated mild steel surface. The embedded smart nanocontainers were homogeneously distributed throughout the coating without major agglomeration, verifying the high affinity between smart nanocontainers and aqueous epoxy coating constituents. Thus, the average grain size of MWCNTs-EG/AgNPs particles within the coating matrix is 112.231 nm, while the average thickness of the modified coating is increased to 14.13 μm in comparison to 13.84 μm of pure coating as depicted in Fig. 12(c).

### 3.9. Self-Healing mechanism

The healing mechanism for MWCNTs-EG/AgNPs compounds was depicted in Fig. 17. The reactions of the anodic and cathodic will begin once the NaCl from seawater reaches the mild steel surface according to the following reactions [48]:

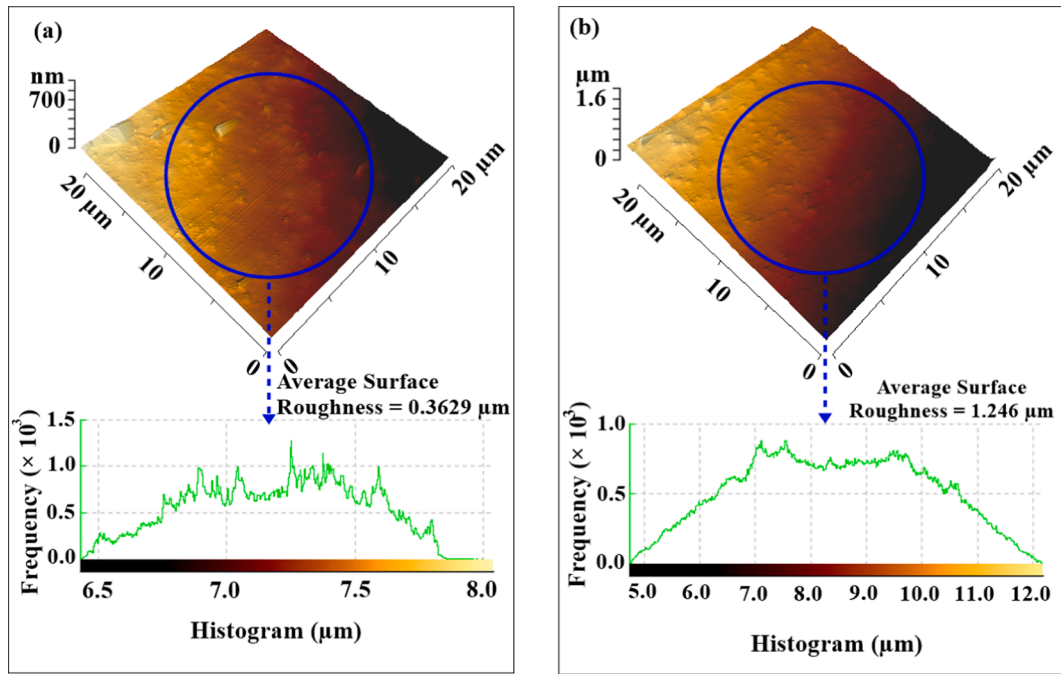


Fig. 15. AFM images of mild steel surface with (a) blank and (b) MWCNTs-EG/AgNPs modified epoxy coating.

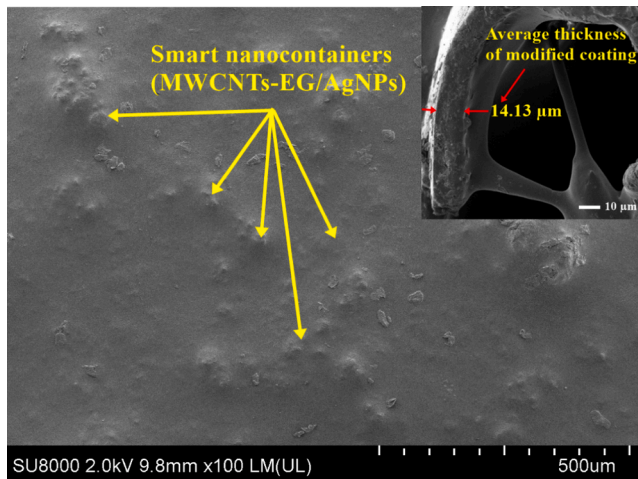
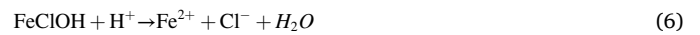
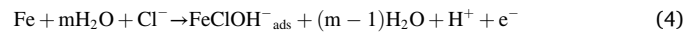


Fig. 16. FESEM image of smart materials coated mild steel surface.

The anodic reaction:



The cathodic reaction:



The presence of NaCl from seawater led to accelerating all the anodic and cathodic reactions which are mainly affected by chloride ions. Noteworthy, when the epoxy coating suffers deterioration, the chloride ions reach the mild steel coupon, resulting in the corrosion products filled the scratch area (Fig. 17). As a consequence of this, the corrosion

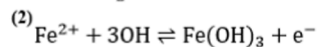
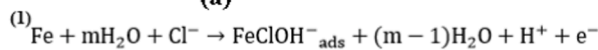
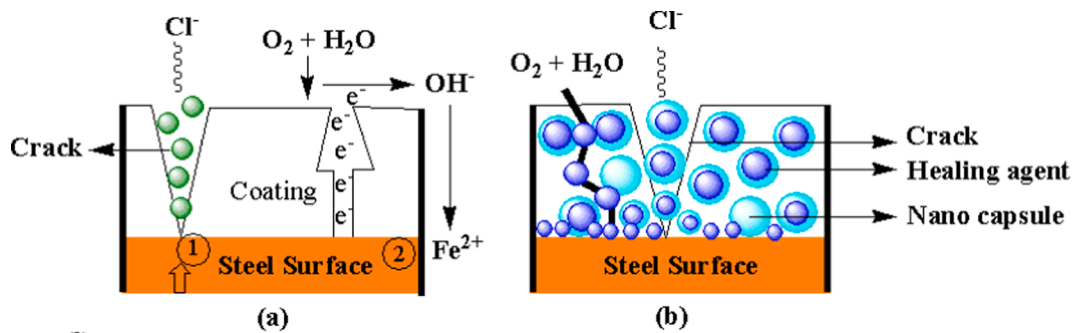


Fig. 17. Corrosion and self-healing mechanisms in the (a) absence and (b) presence of MWCNTs-EG/AgNPs.

process begins, and it is paired with anodic dissolution and cathodic oxygen reduction. Bonding between smart coating and the inhibitor has been established and developed when the mild steel is exposed to an aggressive medium. These bonds are sensitive to the hydroxide ions ( $\text{OH}^-$ ) which are among the main by-products of the metallic corrosion process. The  $\text{OH}^-$  ions facilitate a rise in the pH values of the micro-cathode regions. In turn, this causes the smart coating – inhibitor bond to break, and thus releasing the inhibitor that has negative charges to raise the adhesion force in the direction of the area which has sustained damage. This phenomenon is attributed to increasing the surface activity of EG/AgNPs in the seawater medium and improving the adsorption of inhibitor molecules on the mild steel surface, hence, the EG/AgNPs inhibitor blocking the diffusion paths of chloride ions inside the coating matrix to reach the mild steel surface. It should be noted that the efficacy of green corrosion inhibitor is associated with the presence of polar functions including O, N, or S atoms which are considered the main source of the adsorption process [23].

It should be remembered here that the detection of 12.9% of O atoms in the presence of green inhibitor molecules as shown in Fig. 6 is confirmed the adsorption process of the EG/AgNPs inhibitor. This is closely aligned with the EIS results pertaining to the mild steel coupons characterised by artificial defective areas.

In short, EG/AgNPs behaves as an inhibitor of ferrous metals. This stems from the emergence of covalent bonds between the metal and the lone pair of electrons that inhabit the oxygen atom. Thus, any area of the coating that is damaged undergoes rapid healing by the formation of a passive layer on the mild steel substrate. Consequently, the green EG/AgNPs inhibitor wrapped the area of the defect and prevented the mild steel surface from the direct exposure of aggressive mediums, hence protected the surface against degradation from corrosion.

#### 4. Conclusion

The anti-corrosion behaviour of EG/AgNPs included and epoxy embedded MWCNTs- hybrid material nanocontainers was inspected using standard corrosion monitoring techniques. Nanocontainers, which encapsulated with green EG/AgNPs as corrosion inhibitor was synthesised successfully via a simple and innovative technique. These nanocontainers were applied on the mild steel surface to determine the feasibility of self-healing and anticorrosion inhibition of mild steel surface exposed to aggressive seawater environment. Specimens were thoroughly characterised via FESEM, AFM, TGA, TEM, EDX, and XRD analysis. The SEM analysis was verified that the loaded green (EG/AgNPs) inhibitor in MWCNTs nanocontainers effectively released following the structural damage of coating. The self-healing response affected by the inhibitor release was noticeable in the corrosion resistance measurements on scratched mild steel. Specimens were examined by EIS and polarisation resistance measurements, which are exhibited high inhibition efficiency around 98% and a corrosion rate of 0.009 mm/year in the presence of EG/AgNPs inhibitor. Immersion test results demonstrated a self-healing capability when the coating was deliberately damaged by external mechanical action and this response was attributed to the release of the corrosion inhibitor. The uniformly distributed intelligent nanocontainers were discerned to promote the anticorrosion performance and contribute an essential mechanism in the support of self-healing capabilities for mild steel submerged in seawater. Based on the admirable results, it was established that such smart coating can provide improved corrosion resistance performance of mild steel upon submersion in seawater.

#### CRedit authorship contribution statement

**Mohammad Ali Asaad:** Conceptualization, Methodology, Writing – original draft. **Pandian Bothi Raja:** Formal analysis, Methodology. **Ghasan Fahim Huseien:** Conceptualization, Methodology, Project administration, Supervision. **Roman Fediuk:** Validation, Visualization.

**Mohammad Ismail:** Data curation, Formal analysis. **Rayed Alyousef:** Formal analysis, Validation.

#### Declaration of Competing Interest

The authors declare that they have no known competing financial interests or personal relationships that could have appeared to influence the work reported in this paper.

#### Acknowledgments

The authors gratefully acknowledge the support for this research from Ministry of Higher Education Grant No. 4S090 and (RMC) Research Management Centre Universiti Teknologi Malaysia Grant 16H94, Malaysia. Also, the authors gratefully acknowledges the support of Iraq University College, Iraq and Ministry of Higher Education, Prince Sattam bin Abdulaziz University, Alkharij, Saudi Arabia.

#### References

- [1] T. Śliwa, M. Kruszewski, A. Zare, M. Assadi, A. Sapińska-Śliwa, Potential application of vacuum insulated tubing for deep borehole heat exchangers, *Geothermics* 75 (2018) 58–67.
- [2] L. Yohai, M. Vázquez, M.B. Valcarce, Phosphate ions as corrosion inhibitors for reinforcement steel in chloride-rich environments, *Electrochim. Acta* 102 (2013) 88–96.
- [3] G.S. Duffó, S.B. Farina, Development of an embeddable sensor to monitor the corrosion process of new and existing reinforced concrete structures, *Constr. Build. Mater.* 23 (8) (2009) 2746–2751.
- [4] Z. Panossian, N.L.d. Almeida, R.M.F.D. Sousa, G.D.S. Pimenta, L.B.S. Marques, Corrosion of carbon steel pipes and tanks by concentrated sulfuric acid: a review, *Corros. Sci.* 58 (2012) 1–11.
- [5] T.M. Rao, R. Punathil Meethal, M.S. Amrutha, R. Srinivasan, Studies on group IV and V valve metal corrosion in acidic fluoride media, *J. Electrochem. Soc.* 167 (8) (2020) 081505, <https://doi.org/10.1149/1945-7111/ab8bfa>.
- [6] G. Ji, S. Anjum, S. Sundaram, R. Prakash, Musa paradisica peel extract as green corrosion inhibitor for mild steel in HCl solution, *Corros. Sci.* 90 (2015) 107–117.
- [7] Q.B. Zhang, Y.X. Hua, Corrosion inhibition of mild steel by alkylimidazolium ionic liquids in hydrochloric acid, *Electrochim. Acta* 54 (6) (2009) 1881–1887.
- [8] L.T. Popoola, A.S. Grema, G.K. Latinwo, B. Gutti, A.S. Balogun, Corrosion problems during oil and gas production and its mitigation, *Int. J. Ind. Chem.* 4 (1) (2013) 1–15.
- [9] R. Liu, L. Jiang, J. Xu, C. Xiong, Z. Song, Influence of carbonation on chloride-induced reinforcement corrosion in simulated concrete pore solutions, *Constr. Build. Mater.* 56 (2014) 16–20.
- [10] A. Campos, C.M. López, A. Aguado, Diffusion–reaction model for the internal sulfate attack in concrete, *Constr. Build. Mater.* 102 (2016) 531–540.
- [11] O. Gutierrez, G. Sudarjanto, G. Ren, R. Ganigué, G. Jiang, Z. Yuan, Assessment of pH shock as a method for controlling sulfide and methane formation in pressure main sewer systems, *Water Res.* 48 (2014) 569–578.
- [12] K. De Baere, H. Verstraelen, P. Rigo, S. Van Passel, S. Lenaerts, G. Potters, Reducing the cost of ballast tank corrosion: an economic modeling approach, *Mar. Struct.* 32 (2013) 136–152.
- [13] U. Riaz, C. Nwaoha, S.M. Ashraf, Recent advances in corrosion protective composite coatings based on conducting polymers and natural resource derived polymers, *Prog. Org. Coat.* 77 (4) (2014) 743–756.
- [14] G. Jiang, J. Keller, P.L. Bond, Z. Yuan, Predicting concrete corrosion of sewers using artificial neural network, *Water Res.* 92 (2016) 52–60.
- [15] M.H. Hussin, M.J. Kassim, Electrochemical studies of mild steel corrosion inhibition in aqueous solution by *Uncaria gambir* extract, *J. Phys. Sci.* 21 (1) (2010) 1–9.
- [16] G. Song, N. Ma, H.-N. Li, Applications of shape memory alloys in civil structures, *Eng. Struct.* 28 (9) (2006) 1266–1274.
- [17] Y. Reda, A.M. El-Shamy, K.M. Zohdy, A.K. Eessaa, Instrument of chloride ions on the pitting corrosion of electroplated steel alloy 4130, *Ain Shams Eng. J.* 11 (1) (2020) 191–199.
- [18] J. Han, Y. Yang, S. Nestic, B.N. Brown, Roles of passivation and galvanic effects in localized CO<sub>2</sub> corrosion of mild steel, *CORROSION* 2008, OnePetro, 2008.
- [19] G. Qiao, B. Guo, J. Ou, F. Xu, Z. Li, Numerical optimization of an impressed current cathodic protection system for reinforced concrete structures, *Constr. Build. Mater.* 119 (2016) 260–267.
- [20] R. Subasri, T. Shinohara, Investigations on SnO<sub>2</sub>-TiO<sub>2</sub> composite photoelectrodes for corrosion protection, *Electrochem. Commun.* 5 (10) (2003) 897–902.
- [21] H. Yeganeh, M.A. Shamekhi, Novel polyurethane insulating coatings based on polyhydroxyl compounds, derived from glycolysed PET and castor oil, *J. Appl. Polym. Sci.* 99 (3) (2006) 1222–1233.
- [22] M. Jalilian, H. Yeganeh, M.N. Haghghi, Preparation and characterization of polyurethane electrical insulating coatings derived from novel soybean oil-based polyol, *Polym. Adv. Technol.* 21 (2) (2010) 118–127.

- [23] H. Bentrach, Y. Rahali, A. Chala, Gum Arabic as an eco-friendly inhibitor for API 5L X42 pipeline steel in HCl medium, *Corros. Sci.* 82 (2014) 426–431.
- [24] M. Faustini, A. Maciuk, P. Salvin, C. Roos, M. Lebrini, Corrosion inhibition of C38 steel by alkaloids extract of *Geissospermum laeve* in 1M hydrochloric acid: Electrochemical and phytochemical studies, *Corros. Sci.* 92 (2015) 287–300.
- [25] M.A. Asaad, M. Ismail, P.B. Raja, N.H.A. Khalid, *Rhizophora apiculata* as eco-friendly inhibitor against mild steel corrosion in 1 M HCl, *Surf. Rev. Lett.* 24 (8) (2017) 1–11.
- [26] M.A. Asaad, M.N. Hussein, A.T. Saleh, Corrosion inhibitors for reinforced concrete structures exposed to aggressive environments: a review, *Int. Res. J. Modernization Eng. Technol. Sci.* 03 (02) (2021) 19–27.
- [27] A. Davoodi, S. Honarbaksh, G.A. Farzi, Evaluation of corrosion resistance of polypyrrole/functionalized multi-walled carbon nanotubes composite coatings on 60Cu–40Zn brass alloy, *Prog. Org. Coat.* 88 (2015) 106–115.
- [28] T.T.X. Hang, T.A. Truc, M.-G. Olivier, C. Vandermiers, N. Guérin, N. Pébère, Corrosion protection mechanisms of carbon steel by an epoxy resin containing indole-3 butyric acid modified clay, *Prog. Org. Coat.* 69 (4) (2010) 410–416.
- [29] D.G. Shchukin, M. Zheludkevich, K. Yasakau, S. Lamaka, M.G.S. Ferreira, H. Möhwald, Layer-by-layer assembled nanocontainers for self-healing corrosion protection, *Adv. Mater.* 18 (13) (2006) 1672–1678.
- [30] D.V. Andreeva, D. Fix, H. Möhwald, D.G. Shchukin, Self-healing anticorrosion coatings based on pH-sensitive polyelectrolyte/inhibitor sandwichlike nanostructures, *Adv. Mater.* 20 (14) (2008) 2789–2794.
- [31] M.L. Zheludkevich, J. Tedim, M.G.S. Ferreira, “Smart” coatings for active corrosion protection based on multi-functional micro and nanocontainers, *Electrochim. Acta* 82 (2012) 314–323.
- [32] B.M. Bailey, Y. Leterrier, S.J. Garcia, S. van der Zwaag, V. Michaud, Electrically conductive self-healing polymer composite coatings, *Prog. Org. Coat.* 85 (2015) 189–198.
- [33] H. Choi, K.Y. Kim, J.M. Park, Encapsulation of aliphatic amines into nanoparticles for self-healing corrosion protection of steel sheets, *Prog. Org. Coat.* 76 (10) (2013) 1316–1324.
- [34] M.-R. Yuan, J.-T. Lu, G. Kong, C.-S. Che, Self healing ability of silicate conversion coatings on hot dip galvanized steels, *Surf. Coat. Technol.* 205 (19) (2011) 4507–4513.
- [35] A.H. Jafari, S.M.A. Hosseini, E. Jamalizadeh, Investigation of smart nanocapsules containing inhibitors for corrosion protection of copper, *Electrochim. Acta* 55 (28) (2010) 9004–9009.
- [36] S. Radhakrishnan, C.R. Siju, D. Mahanta, S. Patil, G. Madras, Conducting polyaniline–nano-TiO<sub>2</sub> composites for smart corrosion resistant coatings, *Electrochim. Acta* 54 (4) (2009) 1249–1254.
- [37] E. Abdullayev, R. Price, D. Shchukin, Y. Lvov, Halloysite tubes as nanocontainers for anticorrosion coating with benzotriazole, *ACS Appl. Mater. Interfaces* 1 (7) (2009) 1437–1443.
- [38] C. Ávila-Gonzalez, R. Cruz-Silva, C. Menchaca, S. Sepulveda-Guzman, J. Uruchurtu, Use of silica tubes as nanocontainers for corrosion inhibitor storage, *J. Nanotechnol.* 2011 (2011) 1–9.
- [39] M.F. Montemor, D.V. Snihirova, M.G. Taryba, S.V. Lamaka, I.A. Kartsonakis, A. C. Balakas, G.C. Kordas, J. Tedim, A. Kuznetsova, M.L. Zheludkevich, M.G. S. Ferreira, Evaluation of self-healing ability in protective coatings modified with combinations of layered double hydroxides and cerium molybdate nanocontainers filled with corrosion inhibitors, *Electrochim. Acta* 60 (2012) 31–40.
- [40] S. Lee, G.H. Seo, S. Lee, U. Jeong, S.J. Lee, S.J. Kim, W. Choi, Layer-by-layer carbon nanotube coatings for enhanced pool boiling heat transfer on metal surfaces, *Carbon* 107 (2016) 607–618.
- [41] A. Gergely, Z. Pászti, J. Mihály, E. Drotár, T. Török, Galvanic function of zinc-rich coatings facilitated by percolating structure of the carbon nanotubes. Part II: Protection properties and mechanism of the hybrid coatings, *Prog. Organ. Coat.* 77 (2) (2014) 412–424.
- [42] A. Gergely, Z. Pászti, J. Mihály, E. Drotár, T. Török, Galvanic function of zinc-rich coatings facilitated by percolating structure of the carbon nanotubes. Part I: Characterization of the nano-size particles, *Prog. Organ. Coat.* 78 (2015) 437–445.
- [43] A. Gergely, Z. Pászti, O. Hakkel, E. Drotár, J. Mihály, E. Kálmán, Corrosion protection of cold-rolled steel with alkyd paint coatings composited with submicron-structure types polypyrrole-modified nano-size alumina and carbon nanotubes, *Mater. Sci. Eng., B* 177 (18) (2012) 1571–1582.
- [44] G. Lanzara, Y. Yoon, H. Liu, S. Peng, W.-I. Lee, Carbon nanotube reservoirs for self-healing materials, *Nanotechnology* 20 (33) (2009) 335704, <https://doi.org/10.1088/0957-4484/20/33/335704>.
- [45] S. Park, M. Shon, Effects of multi-walled carbon nano tubes on corrosion protection of zinc rich epoxy resin coating, *J. Ind. Eng. Chem.* 21 (2015) 1258–1264.
- [46] W. Shen, L. Feng, X. Liu, H. Luo, Z. Liu, P. Tong, W. Zhang, Multiwalled carbon nanotubes-reinforced epoxy hybrid coatings with high electrical conductivity and corrosion resistance prepared via electrostatic spraying, *Prog. Org. Coat.* 90 (2016) 139–146.
- [47] A. Madhan Kumar, Z.M. Gasem, In situ electrochemical synthesis of polyaniline/f-MWCNT nanocomposite coatings on mild steel for corrosion protection in 3.5% NaCl solution, *Prog. Org. Coat.* 78 (2015) 387–394.
- [48] F. Daneshvar-Fatah, F. Nasirpour, A study on electrodeposition of Ni-noncovalently treated carbon nanotubes nanocomposite coatings with desirable mechanical and anti-corrosion properties, *Surf. Coat. Technol.* 248 (2014) 63–73.
- [49] A.P. More, S.T. Mhaske, Anticorrosive coating of polyesteramide resin by functionalized ZnO–Al<sub>2</sub>O<sub>3</sub>–Fly ash composite and functionalized multiwalled carbon nanotubes, *Prog. Org. Coat.* 99 (2016) 240–250.
- [50] R.P.S. Chakradhar, G. Prasad, P. Bera, C. Anandan, Stable superhydrophobic coatings using PVDF–MWCNT nanocomposite, *Appl. Surf. Sci.* 301 (2014) 208–215.
- [51] B.P. Singh, S. Samal, S. Nayak, S.M. Majhi, L. Besra, S. Bhattacharjee, The production of a multi-walled carbon nanotube/hexamethylene diisocyanate nanocomposite coating on copper by electrophoretic deposition, *Surf. Coat. Technol.* 206 (6) (2011) 1319–1326.
- [52] R. Karslioglu, H. Akbulut, Comparison microstructure and sliding wear properties of nickel–cobalt/CNT composite coatings by DC, PC and PRC current electrodeposition, *Appl. Surf. Sci.* 353 (2015) 615–627.
- [53] B. Zeybek, E. Aksun, A. Üge, Investigation of corrosion protection performance of poly(N-methylpyrrole)-dodecylsulfate/multi-walled carbon nanotubes composite coatings on the stainless steel, *Mater. Chem. Phys.* 163 (2015) 11–23.
- [54] M. Nasrollahzadeh, S. Mohammad Sajadi, F. Babaei, M. Maham, *Euphorbia helioscopia* Linn as a green source for synthesis of silver nanoparticles and their optical and catalytic properties, *J. Colloid Interface Sci.* 450 (2015) 374–380.
- [55] M.J. Ahmed, G. Murtaza, A. Mehmood, T.M. Bhatti, Green synthesis of silver nanoparticles using leaves extract of *Skimmia laureola*: Characterization and antibacterial activity, *Mater. Lett.* 153 (2015) 10–13.
- [56] K.L. Niraimathi, V. Sudha, R. Lavanya, P. Brindha, Biosynthesis of silver nanoparticles using *Alternanthera sessilis* (Linn.) extract and their antimicrobial, antioxidant activities, *Colloids Surf., B* 102 (2013) 288–291.
- [57] M.A. Asaad, M. Ismail, M.M. Tahir, G.F. Huseien, P.B. Raja, Y.P. Asmara, Enhanced corrosion resistance of reinforced concrete: Role of emerging eco-friendly *Elaeis guineensis*/silver nanoparticles inhibitor, *Constr. Build. Mater.* 188 (2018) 555–568.
- [58] R. Fediuk, M.A. Valery Lesovik, M.A. Asaad, Effect of polymineral systems and disperse reinforcement on self-compacting fibre concrete, *Mag. Concr. Res.* 1900447 (2021) 1–17.
- [59] T. Mochochoko, O.S. Oluwafemi, D.N. Jumbam, S.P. Songca, Green synthesis of silver nanoparticles using cellulose extracted from an aquatic weed; water hyacinth, *Carbohydr. Polym.* 98 (1) (2013) 290–294.
- [60] P.P.N. Vijay Kumar, S.V.N. Pammi, P. Kollu, K.V.V. Satyanarayana, U. Shameem, Green synthesis and characterization of silver nanoparticles using *Boerhaavia diffusa* plant extract and their anti bacterial activity, *Ind. Crops Prod.* 52 (2014) 562–566.
- [61] P. Logeswari, S. Silambarasan, J. Abraham, Ecofriendly synthesis of silver nanoparticles from commercially available plant powders and their antibacterial properties, *Scientia Iranica* 20 (3) (2013) 1049–1054.
- [62] D.A. Kumar, V. Palanichamy, S.M. Roopan, Green synthesis of silver nanoparticles using *Alternanthera dentata* leaf extract at room temperature and their antimicrobial activity, *Spectrochim. Acta Part A Mol. Biomol. Spectrosc.* 127 (2014) 168–171.
- [63] Y.-y. Mo, Y.-k. Tang, S.-y. Wang, J.-m. Lin, H.-b. Zhang, D.-y. Luo, Green synthesis of silver nanoparticles using eucalyptus leaf extract, *Mater. Lett.* 144 (2015) 165–167.
- [64] D.R. Raj, S. Prasanth, T. Vineeshkumar, S. Sudarsanakumar, Surface plasmon resonance based fiber optic dopamine sensor using green synthesized silver nanoparticles, *Sens. Actuators, B* 224 (2016) 600–606.
- [65] V.K. Sharma, R.A. Yngard, Y. Lin, Silver nanoparticles: green synthesis and their antimicrobial activities, *Adv. Colloid Interface Sci.* 145 (1) (2009) 83–96.
- [66] N.G. Bastús, F. Merçoçi, J. Piella, V. Puntes, Synthesis of highly monodisperse citrate-stabilized silver nanoparticles of up to 200 nm: kinetic control and catalytic properties, *Chem. Mater.* 26 (9) (2014) 2836–2846.
- [67] P. Cheviron, F. Gouanvé, E. Espuche, Green synthesis of colloid silver nanoparticles and resulting biodegradable starch/silver nanocomposites, *Carbohydr. Polym.* 108 (2014) 291–298.
- [68] S. Yang, P. Liu, Y. Zhang, Q.-N. Guo, Y. Chen, Effects of silver nanoparticles size and shape on light scattering, *Optik* 127 (14) (2016) 5722–5728.
- [69] C. Dong, X. Zhang, H. Cai, C. Cao, Green synthesis of biocompatible silver nanoparticles mediated by *Osmanthus fragrans* extract in aqueous solution, *Optik* 127 (22) (2016) 10378–10388.
- [70] Z. Abboud, S. Vivekanandhan, M. Misra, A.K. Mohanty, Leaf extract mediated biogenic process for the decoration of graphene with silver nanoparticles, *Mater. Lett.* 178 (2016) 115–119.
- [71] I. Khalid, O. Sulaiman, R. Hashim, W. Razak, N. Jumhuri, M.S.M. Rasat, Evaluation on layering effects and adhesive rates of laminated compressed composite panels made from oil palm (*Elaeis guineensis*) fronds, *Mater. Des.* 68 (2015) 24–28.
- [72] K. Szymona, P. Borysiuk, P.S. H’ng, K.L. Chin, M. Mamiński, Valorization of waste oil palm (*Elaeis guineensis* Jacq.) biomass through furfurylation, *Mater. Des.* 53 (2014) 425–429.
- [73] S.K. Chang, A. Ismail, T. Yanagita, N. Mohd Esa, M.T.H. Baharuldin, Antioxidant peptides purified and identified from the oil palm (*Elaeis guineensis* Jacq.) kernel protein hydrolysate, *J. Funct. Foods* 14 (2015) 63–75.
- [74] S. Kok, M. Ong-Abdullah, G.C. Ee, P. Namasivayam, Comparison of nutrient composition in kernel of tenera and clonal materials of oil palm (*Elaeis guineensis* Jacq.), *Food Chem.* 129 (4) (2011) 1343–1347.
- [75] V. Soundararajan, S. Sreenivasan, Antioxidant activity of *elaeis guineensis* leaf extract: an alternative nutraceutical approach in impeding aging, *APCBEE Procedia* 2 (2012) 153–159.
- [76] H.H.H. Hefni, E.M. Azzam, E.A. Badr, M. Hussein, S.M. Tawfik, Synthesis, characterization and anticorrosion potentials of chitosan-g-PEG assembled on silver nanoparticles, *Int. J. Biol. Macromol.* 83 (2016) 297–305.

- [77] A.M. Atta, H.A. Allohedan, G.A. El-Mahdy, A.R.O. Ezzat, Application of stabilized silver nanoparticles as thin films as corrosion inhibitors for carbon steel alloy in 1 M hydrochloric acid, *J. Nanomater.* 2013 (2013).
- [78] M.M. Solomon, S.A. Umoren, In-situ preparation, characterization and anticorrosion property of polypropylene glycol/silver nanoparticles composite for mild steel corrosion in acid solution, *J. Colloid Interface Sci.* 462 (2016) 29–41.
- [79] M.M. Solomon, H. Gerengi, T. Kaya, S.A. Umoren, Enhanced corrosion inhibition effect of chitosan for St37 in 15% H<sub>2</sub>SO<sub>4</sub> environment by silver nanoparticles, *Int. J. Biol. Macromol.* 104 (2017) 638–649.
- [80] E.M.S. Azzam, A.A. Abd El-Aal, Corrosion inhibition efficiency of synthesized poly 12-(3-amino phenoxy) dodecane-1-thiol surfactant assembled on silver nanoparticles, *Egypt. J. Pet.* 22 (2) (2013) 293–303.
- [81] M. Akbarian, M.E. Olya, M. Mahdavian, M. Ataefard, Effects of nanoparticulate silver on the corrosion protection performance of polyurethane coatings on mild steel in sodium chloride solution, *Prog. Org. Coat.* 77 (8) (2014) 1233–1240.
- [82] M.M. Solomon, S.A. Umoren, E.J. Abai, Poly(methacrylic acid)/silver nanoparticles composites: In-situ preparation, characterization and anticorrosion property for mild steel in H<sub>2</sub>SO<sub>4</sub> solution, *J. Mol. Liq.* 212 (2015) 340–351.
- [83] M.M. Solomon, H. Gerengi, S.A. Umoren, N.B. Essien, U.B. Essien, E. Kaya, Gum Arabic-silver nanoparticles composite as a green anticorrosive formulation for steel corrosion in strong acid media, *Carbohydr. Polym.* 181 (2018) 43–55.
- [84] P. Jain, B. Patidar, J. Bhawar, Potential of nanoparticles as a corrosion inhibitor: a review, *J. Bio-and Tribo-Corros.* 6 (2) (2020) 1–12.
- [85] K.K. Alaneme, S.J. Olusegun, O.T. Adelowo, Corrosion inhibition and adsorption mechanism studies of *Hunteria umbellata* seed husk extracts on mild steel immersed in acidic solutions, *Alexandria Eng. J.* 55 (1) (2016) 673–681.
- [86] E. Kowsari, M. Payami, R. Amini, B. Ramezanzadeh, M. Javanbakht, Task-specific ionic liquid as a new green inhibitor of mild steel corrosion, *Appl. Surf. Sci.* 289 (2014) 478–486.
- [87] A.I. Ali, Melia azedarach L as eco- friendly corrosion inhibitor for Aluminum in 2M HCl, *J. Mater. Environ. Sci.* 5 (3) (2014) 793–802.
- [88] R. Lemus-Mondaca, A. Vega-Gálvez, P. Rojas, K. Stucken, C. Delporte, G. Valenzuela-Barra, R.J. Jagus, M.V. Agüero, A. Pasten, Antioxidant, antimicrobial and anti-inflammatory potential of *Stevia rebaudiana* leaves: effect of different drying methods, *J. Appl. Res. Med. Aromat. Plants* 11 (2018) 37–46.
- [89] R. Mariselvam, A. Ranjitsingh, A.U.R. Nanthini, K. Kalirajan, C. Padmalatha, P. M. Selvakumar, Green synthesis of silver nanoparticles from the extract of the inflorescence of *Cocos nucifera* (Family: Arecaceae) for enhanced antibacterial activity, *Spectrochim. Acta Part A Mol. Biomol. Spectrosc.* 129 (2014) 537–541.
- [90] I.A. Kartsonakis, L.L. Danilidis, G.S. Pappas, G.C. Kordas, Encapsulation and Release of Corrosion Inhibitors into Titania Nanocontainers, *J. Nanosci. Nanotechnol.* 10 (9) (2010) 5912–5920.
- [91] S. Radhakrishnan, C.R. Siju, D. Mahanta, S. Patil, G. Madras, Conducting polyaniline-nano-TiO<sub>2</sub> composites for smart corrosion resistant coatings, *Electrochim. Acta* 54 (4) (2009) 1249–1254.
- [92] E.A.K. Nivethaa, S. Dhanavel, V. Narayanan, A. Stephen, Fabrication of chitosan/MWCNT nanocomposite as a carrier for 5-fluorouracil and a study of the cytotoxicity of 5-fluorouracil encapsulated nanocomposite towards MCF-7, *Polym. Bull.* 73 (11) (2016) 3221–3236.
- [93] L. Bao, W. Zhang, X. Zhang, Y. Chen, S. Chen, L. Wu, R. Shen, Y. Ye, Impact of MWCNT/Al on the combustion behavior of hydroxyl ammonium nitrate (HAN)-based electrically controlled solid propellant, *Combust. Flame* 218 (2020) 218–228.
- [94] M.E. Jancy, L. Inbathamizh, Green synthesis and characterization of nano silver using leaf extract of *Morinda pubescens*, *Asian J. Pharm. Clin. Res.* 5 (2012) 159–162.
- [95] J. Yoon, X. Cao, Q. Zhou, L.Q. Ma, Accumulation of Pb, Cu, and Zn in native plants growing on a contaminated Florida site, *Sci. Total Environ.* 368 (2–3) (2006) 456–464.
- [96] M. Krzesłowska, I. Rabęda, A. Basińska, M. Lewandowski, E.J. Mellerowicz, A. Napieralska, Sławomir Samardakiewicz, A. Woźny, Pectin cell wall thickenings formation—A common defense strategy of plants to cope with Pb, *Environ. Pollut.* 214 (2016) 354–361.
- [97] J. Pichtel, K. Kuroiwa, H.T. Sawyerr, Distribution of Pb, Cd and Ba in soils and plants of two contaminated sites, *Environ. Pollut.* 110 (1) (2000) 171–178.
- [98] Y. Raghupathy, A. Kamboj, M.Y. Rekha, N.P. Narasimha Rao, C. Srivastava, Copper-graphene oxide composite coatings for corrosion protection of mild steel in 3.5% NaCl, *Thin Solid Films* 636 (2017) 107–115.
- [99] P. Khodaei, M. Shabani-Nooshabadi, M. Behpour, Epoxy-based nanocomposite coating reinforced by a zeolite complex: Its anticorrosion properties on mild steel in 3.5 wt% NaCl media, *Prog. Org. Coat.* 136 (2019) 105254, <https://doi.org/10.1016/j.porgcoat.2019.105254>.
- [100] Bülent Zeybek, E. Aksun, A. Üge, Investigation of corrosion protection performance of poly (N-methylpyrrole)-dodecylsulfate/multi-walled carbon nanotubes composite coatings on the stainless steel, *Mater. Chem. Phys.* 163 (2015) 11–23.
- [101] K. Kamaraj, R. Devarapalli, T. Siva, S. Sathiyarayanan, Self-healing electrosynthesized polyaniline film as primer coat for AA 2024–T3, *Mater. Chem. Phys.* 153 (2015) 256–265.
- [102] A. Phanasgaonkar, V.S. Raja, Influence of curing temperature, silica nanoparticles and cerium on surface morphology and corrosion behaviour of hybrid silane coatings on mild steel, *Surf. Coat. Technol.* 203 (16) (2009) 2260–2271.
- [103] W. Yang, W. Feng, Z. Liao, Y. Yang, G. Miao, B. Yu, X. Pei, Protection of mild steel with molecular engineered epoxy nanocomposite coatings containing corrosion inhibitor functionalized nanoparticles, *Surf. Coat. Technol.* 406 (2021) 126639, <https://doi.org/10.1016/j.surfcoat.2020.126639>.
- [104] P.K. Jaseela, M. Kuruvilla, L. Williams, C. Jacob, K.O. Shamsheera, A. Joseph, Excellent protection of mild steel in sodium chloride solution for a substantial period of time using a hybrid nanocoating of poly vinyl alcohol and Titania, *Arabian J. Chem.* 13 (8) (2020) 6921–6930.
- [105] P. Mourya, S. Banerjee, M.M. Singh, Corrosion inhibition of mild steel in acidic solution by *Tagetes erecta* (Marigold flower) extract as a green inhibitor, *Corros. Sci.* 85 (2014) 352–363.
- [106] A.Y. El-Etre, A.I. Ali, A novel green inhibitor for C-steel corrosion in 2.0 mol-L –1 hydrochloric acid solution, *Chin. J. Chem. Eng.* 25 (3) (2017) 373–380.
- [107] M. Ali Asaad, N.N. Sarbini, A. Sulaiman, M. Ismail, G.F. Huseien, Z. Abdul Majid, P. Bothi Raja, Improved corrosion resistance of mild steel against acid activation: impact of novel *Elaeis guineensis* and silver nanoparticles, *J. Ind. Eng. Chem.* 63 (2018) 139–148.
- [108] O. Kazum, M.B. Kannan, N. Scharnagl, C. Blawert, Y.H. He, Electrochemical corrosion behaviour of WE54 magnesium alloy, *Trans. Tech. Publ.* 765 (2013) 644–647.
- [109] X. Liu, C. Gu, Z. Wen, B. Hou, Improvement of active corrosion protection of carbon steel by water-based epoxy coating with smart CeO<sub>2</sub> nanocontainers, *Prog. Org. Coat.* 115 (2018) 195–204.
- [110] R. Samiee, B. Ramezanzadeh, M. Mahdavian, E. Alibakhshi, Assessment of the smart self-healing corrosion protection properties of a water-base hybrid organo-silane film combined with non-toxic organic/inorganic environmentally friendly corrosion inhibitors on mild steel, *J. Cleaner Prod.* 220 (2019) 340–356.
- [111] I.A. Wonnice Ma, A. Sh., S. Bashir, S.S. A Kumar, R. K, R. S, Development of active barrier effect of hybrid chitosan/silica composite epoxy-based coating on mild steel surface, *Surf. Interfaces* 25 (2021) 101250, <https://doi.org/10.1016/j.surfint.2021.101250>.
- [112] Y. Feng, Y.F. Cheng, An intelligent coating doped with inhibitor-encapsulated nanocontainers for corrosion protection of pipeline steel, *Chem. Eng. J.* 315 (2017) 537–551.
- [113] H.-K. Song, H.-Y. Hwang, K.-H. Lee, L.H. Dao, The effect of pore size distribution on the frequency dispersion of porous electrodes, *Electrochim. Acta* 45 (14) (2000) 2241–2257.
- [114] L.-Y. Cui, S.-D. Gao, P.-P. Li, R.-C. Zeng, F. Zhang, S.-Q. Li, E.-H. Han, Corrosion resistance of a self-healing micro-arc oxidation/polymethyltrimethoxysilane composite coating on magnesium alloy AZ31, *Corros. Sci.* 118 (2017) 84–95.
- [115] J.A. Syed, S. Tang, X. Meng, Intelligent saline enabled self-healing of multilayer coatings and its optimization to achieve redox catalytically provoked anti-corrosion ability, *Appl. Surf. Sci.* 383 (2016) 177–190.
- [116] T. Siva, S. Sathiyarayanan, Self healing coatings containing dual active agent loaded urea formaldehyde (UF) microcapsules, *Prog. Org. Coat.* 82 (2015) 57–67.
- [117] M. Wang, M. Liu, J. Fu, An intelligent anticorrosion coating based on pH-responsive smart nanocontainers fabricated via a facile method for protection of carbon steel, *J. Mater. Chem. A* 3 (12) (2015) 6423–6431.
- [118] L. Zhai, G. Ling, J. Li, Y. Wang, The effect of nanoparticles on the adhesion of epoxy adhesive, *Mater. Lett.* 60 (25–26) (2006) 3031–3033.